

ERRATUM: SUPER LUMINOUS SUPERNOVAE AS STANDARDIZABLE CANDLES AND HIGH REDSHIFT DISTANCE PROBES

C. INSERRA AND S. J. SMARTT

Astrophysics Research Centre, School of Mathematics and Physics, Queens University Belfast, Belfast BT7 1NN, UK
Draft version October 29, 2021

ABSTRACT

We investigate the use of type Ic Super Luminous Supernovae (SLSN Ic) as standardizable candles and distance indicators. Their appeal as cosmological probes stems from their remarkable peak luminosities, hot blackbody temperatures and bright rest frame ultra-violet emission. We present a sample of sixteen published SLSN, from redshifts 0.1 to 1.2 and calculate accurate K -corrections to determine uniform magnitudes in two synthetic rest frame filter band-passes with central wavelengths at 400nm and 520nm. At 400nm, we find an encouragingly low scatter in their uncorrected, raw mean magnitudes **with** $M(400) = -21.70 \pm 0.47$ **mag** for the full sample of sixteen objects. We investigate the correlation between their decline rates and peak magnitude and find that the brighter events appear to decline more slowly. In a similar manner to the Phillips relation for type Ia SNe, we define a ΔM_{30} **decline relation**. This correlates peak magnitude and decline over **30** days and can reduce the scatter in standardized peak magnitudes to ± 0.25 mag. We further show that $M(400)$ appears to have a strong color dependence. Redder objects are fainter and also become redder faster. Using this peak magnitude - color evolution relation, a **low scatter of between ± 0.19 mag and ± 0.26 mag** can be found in peak magnitudes, depending on sample selection. However we caution that only eight to ten objects currently have enough data to test this peak magnitude - color evolution relation. We conclude that SLSN Ic are promising distance indicators in the high redshift Universe in regimes beyond those possible with SNe Ia. Although the empirical relationships are encouraging, the unknown progenitor systems, how they may evolve with redshift, and the uncertain explosion physics are of some concern. The two major measurement uncertainties are the limited numbers of low redshift, well studied, objects available to test these relationships and internal dust extinction in the host galaxies.

Subject headings: supernovae: general – distance scale

1. INTRODUCTION

In recent years the new generation of deep, wide surveys like the Palomar Transient Factory (PTF, Rau et al. 2009), the Panoramic Survey Telescope & Rapid Response System (Pan-STARRS, Kaiser et al. 2010), the Catalina Real-time Transient Survey (CRTS, Drake et al. 2009), and the La Silla QUEST survey (Baltay et al. 2013) have searched for supernovae (SNe) in the local Universe without a galaxy bias and have found new types of luminous transients. These were preceded by the smaller scale, but pioneering, Texas Supernova Search (Quimby et al. 2005) which uncovered the first SN recognised as “super-luminous” (Quimby 2006; Quimby et al. 2007; Smith et al. 2007). These super-luminous supernovae (hereafter SLSN) are characterised by absolute magnitudes at maximum light of $M_{AB} < -21$ mag and total radiated energies of order 10^{51} ergs. They are factors of 5 to 100 brighter than type Ia SNe or normal core-collapse events. In reviewing the discoveries to date, Gal-Yam (2012) proposed three observational classes for these highly luminous supernovae: SLSN I, SLSN II and SLSN R based on their photometric evolution and presumed physical characteristics.

The SLSN I are hydrogen free and show a blue continuum, a distinctive “W”-shaped spectral feature at ~ 4200 Å and a transformation in their spectra to those of normal type Ic SNe. They were first recognised by

Quimby et al. (2011a), who tied the transients SN2005ap and SCP-06F6 (Quimby et al. 2007; Barbary et al. 2009) together with PTF discoveries by determining their redshifts and common broad photospheric absorption lines. A detailed study of one of the nearer events (SN2010gx/PTF10cwr at $z = 0.23$) by Pastorello et al. (2010a) showed that it spectroscopically evolved into a type Ic SN but on much longer timescales than usual. The possibility of quantitatively studying these at much higher redshifts ($z \sim 1$) than the known supernova population was shown by Chomiuk et al. (2011) in the Pan-STARRS1 Medium Deep field survey. Inserra et al. (2013) recently reported a detailed study of a sample of five nearby SLSN and explored quantitative models to fit the lightcurves. They favoured a model of a spinning down magnetic neutron star as the source of the energy input to power their luminous light curves. This magnetar model for luminous supernovae was theoretically proposed by Kasen & Bildsten (2010), Woosley (2010) and further investigated by Dessart et al. (2012). Since the optical spectra of these SNe evolve to be similar to the normal and more common classes of type Ic SNe, Inserra et al. (2013) simply termed them SLSN Ic.

Gal-Yam (2012) suggested a separate definition of “SLSN R” mostly based on the observed slow lightcurve evolution of SN2007bi (Gal-Yam et al. 2009; Young et al. 2010) and the fact that this slow decline could be explained theoretically by the decay of radioactive ^{56}Ni and ^{56}Co (hence the use of “R”). However, recent studies by

Nicholl et al. (2013) and McCrum et al. (2014a) showed that two SLSN which are very similar to SN2007bi are better explained by the magnetar model. In fact the physical nature of the radioactive powering is not unambiguously established in any of them which means the label of “SLSN R” is not one that is observationally secure. Nicholl et al. (2013) illustrated the similarity in the early spectra of the SLSN I types (of Pastorello et al. 2010a; Quimby et al. 2011a; Inserra et al. 2013) and the SN2007bi-like events (PTF12dam in particular). It is certainly possible the “SLSN I” and the “SLSN R” explosions have the same physical mechanism. However, it is not clear yet if there is a continuum in their decay timescales or if there are two distinct groups which decline with different rates after peak. Following Inserra et al. (2013) and Nicholl et al. (2013), we will use the classification term SLSN Ic to refer to *all* the hydrogen poor super-luminous supernovae. Their physical nature may be debated, but the simple observational term of type Ic is quite secure in the classical scheme of SN classification. In order to distinguish between the two observational groups we will use the terms SN2005ap-like and SN2007bi-like events since these are the prototypes of the faster and slower evolving events known to date.

The SLSN of type II generally show strong H I lines in emission which indicate the interaction of fast moving ejecta with a pre-existing and slower moving shell of material. In this scenario, the kinetic energy of the ejecta (with energies of order 10^{51} ergs) is converted to luminosity during the collision (e.g. Smith & McCray 2007; Agnoletto et al. 2009). These have been relatively easy to identify due to the strong emission line signatures, although there is still uncertain physics concerning the symmetry and clumping of the interacting shells. The interaction model has been extended to explain the hydrogen free SLSN by Chevalier & Irwin (2011) and Ginzburg & Balberg (2012). Benetti et al. (2014) have recently shown that the transient CSS121015:004244+132827 appears quite similar to many of the SLSN Ic of Quimby et al. (2011a) and Inserra et al. (2013) but weak and transitory H α emission is detected, suggestive of interaction occurring.

The number of SLSN Ic which have been discovered and recognised as such has increased rapidly, with discoveries out to redshifts of $z \sim 4$ (Chomiuk et al. 2011; Cooke et al. 2012; Berger et al. 2012; Leloudas et al. 2012; Inserra et al. 2012; Lunnan et al. 2013; Howell et al. 2013; Kostrzewa-Rutkowska et al. 2013; Benetti et al. 2014; McCrum et al. 2014b). They seem to be fairly homogeneous in their spectroscopic and photometric properties and have attracted considerable attention due to their potential utility as cosmological standard candles. The potential lies in the fact that they are 2-3 magnitudes brighter than type Ia SNe and their hot blackbody temperatures mean that their UV continuum emission is detectable at high redshifts in the optical and near-infrared (e.g. Cooke et al. 2012). The study of these objects is still a relatively youthful endeavor as they were first recognised as highly luminous in 2010-11 (Pastorello et al. 2010a; Quimby et al. 2011a; Chomiuk et al. 2011). Quimby et al. (2013b) already pointed out that the peak magnitudes of SLSN Ic may be quite narrowly distributed at $M = -21.7 \pm 0.4$ (in the the unfiltered ROTSE-IIIb band-pass). Detailed investigation of

this issue is now possible with a large sample of well observed SLSN Ic, which have multi-color light-curves and spectral sequences to allow more accurate K -corrections to be determined. King et al. (2014) discussed how novel high redshift standard candles could be used to probe the dark energy equation of state $w(z)$ and how this compares to the current state-of-the-art type Ia supernova and baryon acoustic oscillation measurements. It would appear that a large number ($\sim 10^3$) are required to improve on $w(z)$ estimates, and objects should cover a long redshift baseline, which is challenging. Nevertheless, any additional cosmological probes are potentially useful and their merits should be studied.

In this paper we analyse a sample of well observed SLSN Ic with complete light-curves from before peak to beyond 30 days. We test whether there is any relation between empirical, observable quantities (such as light-curve shape, color evolution and peak luminosity) that could make them useful cosmological standardizable candles. It is well known that absolute magnitudes of type Ia SNe have been standardized using different methods based on their empirical characteristics. The earliest and simplest standardization method correlated peak magnitudes with decline rates and is referred to as the Δm_{15} method (Rust 1974; Pskovskii 1977; Phillips 1993; Hamuy et al. 1996). This gave way to much more sophisticated approaches such as the Multicolor Light Curve Shapes method (MLCS, Riess et al. 1996, 1998), the stretch method (Perlmutter et al. 1997; Goldhaber et al. 2001), the spectral adaptive light curve template method (SALT, Guy et al. 2005, 2007) and the BayeSN method (Mandel et al. 2009, 2011). In the context of this initial attempt to standardize SLSN Ic, it is useful to reflect on the benchmark results from the early attempts with the Δm_{15} method. Phillips (1993) used 9 SNe and illustrated the large dispersion in the raw absolute magnitudes (without any correction) of $\sigma = 0.8, 0.6$ and 0.5 for B, V and I respectively¹. The Phillips Δm_{15} correlation immediately reduced the scatter to $\sigma = 0.36, 0.28$ and 0.38 in BVI . This method was revisited with a much larger sample by Prieto et al. (2006), who produced an rms scatter around the linear fit of $\sigma = 0.17, 0.14$ for 94 SNe in BV and 0.15 for 87 SNe in the I -band. Since that time, the community has been investigating other standardizable candles with a view to reaching similar scatter values. Type II-P SNe have been proposed, which appear to have an rms scatter in their standardizable luminosity-velocity relation of around 0.26 mag (Hamuy & Pinto 2002; Nugent et al. 2006; Poznanski et al. 2009; D’Andrea et al. 2010). Maguire et al. (2010) suggested that going to the near infrared (NIR) could potentially reduce this to 0.1-0.15 mag, although the disadvantage of SNe II-P as distance indicators is that they are 2-3 magnitudes fainter than SNe Ia. We note that also GRB have been suggested to be possible standardizable candle (Cano 2014; Cano & Jakobsson 2014). These attempts illustrate that achieving an rms scatter of 0.1 – 0.3 magnitudes for any new standardizable candle would make it competitive and interesting to study further. This paper

¹ The σ for the raw absolute magnitudes is simply the standard deviation of the population, as calculated by Phillips (1993). The σ or scatter around the best fit line for Δm_{15} is the rms error of the linear fit.

investigates the use of SLSN Ic as such standardizable candles.

2. THE SAMPLE AND DATA

The sample chosen was selected from the published SLSN Ic which have well sampled light-curves around peak luminosity. We required photometric coverage from several days pre-maximum (or a good estimate of the time and value of peak luminosity) to about 35 rest frame days after peak luminosity. We further required photometry in observer frame filters which, after K -correction, had similar equivalent rest frame bandpasses (see Section 4). An accurate spectroscopic redshift is also required to provide reliable relative distances. The redshift distribution of the known population of well observed SLSN ($0.1 \leq z \leq 1.6$) means this selection is not trivial and not all the 30-40 or so known SLSN can be used in our sample calculations (see Lunnan et al. 2014, for an extensive, but not complete, compilation of 31 SLSN). We found sixteen SNe which had suitable data for our analysis: SN2010gx, SN2011kf, SN2011ke, SN2012il, SN2005ap, PS1-10ky, PTF09cnd, SCP-06F6, PTF11rks, PS1-10bj, PS1-10pm, LSQ12dlf, SN2013dg, PS1-11ap, PTF12dam and CSS121015:004244+132827 (with data from Pastorello et al. 2010a; Inserra et al. 2013; Quimby et al. 2007; Barbary et al. 2009; Quimby et al. 2011a; Chomiuk et al. 2011; Lunnan et al. 2013; Nicholl et al. 2013; McCrum et al. 2014a; Benetti et al. 2014; McCrum et al. 2014b; Nicholl et al. 2014). The details are listed in Table 1. We highlight the important caveat that this sample selection does not take potential Malmquist bias into account. The identification process of these targets comes from a range of surveys, each with quite different magnitude limits combined with different selection procedures for selecting targets for spectroscopic follow-up. Hence the process from discovery of a transient to identification as a super-luminous supernova is quite inhomogeneous. It is certainly true that the intrinsically brightest SNe are over represented in magnitude limited surveys compared to their volumetric rates which may introduce a shift in absolute magnitude simply because the lower luminosity events are under-represented. There does appear to be a significant gap between the SLSN Ic and the brightest (and most energetic) of type Ic SNe (e.g. see Inserra et al. 2013, for a comparison). Whether this gap is Malmquist type bias or real remains to be investigated.

Thirteen of these objects appear to be similar to the well observed SN2010gx, and these decay rapidly after peak magnitude. The similarity of their lightcurves and spectral evolution has been discussed by Quimby et al. (2011a), Inserra et al. (2013) and Gal-Yam (2012), amongst others and we label these 2005ap-like since that was the first one discovered. Two of our sample of sixteen (PTF12dam and PS1-11ap) decline on noticeably slower timescales and are similar to SN2007bi (see Section 1). We include them in our analysis for completeness and show results with and without these two events (and refer to them as 2007bi-like). The object CSS121015:004244+132827 (hereafter CSS121015, Benetti et al. 2014), has been classified as a SLSN II since it shows signs of $H\alpha$ that is probably linked to the supernova rather than the host galaxy. We include it here for completeness, since its spectra resembles SN2010gx and

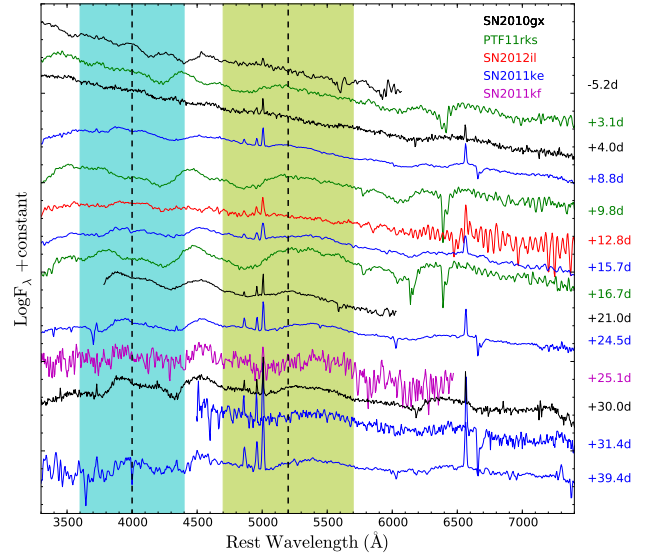


FIG. 1.— General spectral evolution of SLSN Ic (2005ap-like) from 5d before maximum light to 40d after. The phase of each spectrum relative to light curve peak in the rest frame is shown on the right. These restframe spectra have been corrected for Galactic extinction. They have been convolved with a Gaussian function of FWHM = 5 Å and subsequently binned to 5 Å per pixel. The 400nm and 520nm wavebands are shown in cyan and green respectively, with their effective centers marked with black dashed lines. The data are from Pastorello et al. (2010a) and Inserra et al. (2013). Table 1 provides a full list of references to the original sources of data for all objects.

the other SLSN Ic with the addition of weak hydrogen features, and at high redshift one might struggle to see the subtle differences present in spectra. Again, we will show results with and without this event. We note that although we included it and label it a SLSN II, we are not considering the broader and more populous class of SLSN II, such as the SN2006gy-like events. These luminous type II_{in} SNe are unambiguously driven by strong CSM interaction and collisions of hydrogen rich gas and they are observationally very distinct. Hereafter we will refer to three samples. The thirteen 2005ap-like events are called the “pure sample”. Including the two 2007bi-like objects makes an “extended sample” of fifteen objects. And adding in CSS121015 defines the “complete sample” of sixteen objects.

We included all SLSN having enough data to be useful for our analysis. The SLSN published in the literature which are not reported and used here were rejected primarily on the basis that they lack the photometric data required for our careful and uniform analysis. There are at least seven other SLSN Ic which are securely classified in previous work and have data published, but their photometric coverage does not present a complete enough dataset around the epoch of 0-30d (rest-frame) in filters that are suitable for the comparison we undertake in Section 4. These are SN2006oz (Leloudas et al. 2012), PTF09cwl and PTF09atu (Quimby et al. 2011a), PTF10hgi (Inserra et al. 2013), PS1-10awh (Chomiuk et al. 2011), PS1-11bam (Berger et al. 2012) and SSS120810:231802-560926 (Nicholl et al. 2014). We did not consider PS1-10afx further because of the probable nature of it being a lensed type Ia SN and not a SLSN

TABLE 1
 SAMPLE OF SLSN.

SN	z	$E(B-V)$	m	Ref. ^a	Filters 400,520	A_f	$M(400)$	$\Delta M_{10}(400)$	$\Delta M_{20}(400)$	$\Delta M_{30}(400)$	$\Delta M(400-520)_{30}$
SLSN Ic (2005ap-like)											
SN2011ke	0.143	0.01	17.70 (g)	1	g→ 400, r→ 520	0.05	-21.27	0.46	1.22	2.14	0.65
SN2012il	0.175	0.02	18.34 (g)*	1	g→ 400, r→ 520	0.09	-21.31	0.41	1.06	1.74	0.50
PTF11rks	0.190	0.04	19.13 (g)	1	g→ 400, r→ 520	0.17	-20.63	0.28	0.95	2.02	0.95
SN2010gx	0.230	0.04	18.43 (g)	2	g→ 400, r→ 520	0.13	-21.73	0.13	0.63	1.41	0.58
SN2011kf	0.245	0.02	18.60 (g)	1	g→ 400	0.09	-21.76	0.09	0.54	1.25	-
LSQ12dlf	0.255	0.01	18.78 (V)	3	V→ 400, R→ 520	0.03	-21.59	0.38	0.73	1.34	0.55
PTF09cnd	0.258	0.02	18.09 (R)	4	R→ 400	0.05	-22.15	0.19	0.50	0.94	-
SN2013dg	0.265	0.04	19.26 (g)*	3	g→ 400, r→ 520	0.15	-21.38	0.43	1.24	2.00	0.75
SN2005ap	0.283	0.01	18.35 (R)	5	R→ 400	0.02	-22.12	0.19	0.66	-	-
PS1-10bzj	0.650	0.01	21.44 (r)*	6	r→ 400, z→ 520	0.02	-21.11	0.21	0.81	1.55	0.66
PS1-10ky	0.956	0.03	21.27 (i)	7	i→ 400, z→ 520	0.06	-22.07	0.21	0.90	1.31	0.31
SCP-06F6	1.189	0.01	21.04 (z)	8	z→ 400	0.01	-22.17	0.11	0.44	0.90	-
PS1-10pm	1.206	0.02	21.74 (z)	9	z→ 400	0.02	-22.03	0.15	0.43	-	-
SLSN Ic (2007bi-like)											
PTF12dam	0.107	0.01	16.84 (g)*	10	g→ 400, r→ 520	0.04	-21.56	0.02	0.15	0.28	0.08
PS1-11ap	0.524	0.01	20.11 (r)	11	r→ 400, i→ 520	0.02	-21.82	0.09	0.28	0.60	0.11
SLSN II											
CSS121015	0.287	0.08	18.19 (V)	12	V→ 400, R→ 520	0.24	-22.48	0.25	0.76	0.93	0.21

NOTE. — From left to right : SN designation; measured redshift; foreground extinction; observed magnitude (AB system) at peak with the band used in parentheses; reference; observed filters used to calculate the synthetic 400nm and 520nm magnitudes; extinction toward the SN in the observed band; absolute magnitude in the 400nm band, magnitude decrease in 10, 20 and 30 days; the color change between the 400nm and 520nm synthetic bands at peak and 30 days after.

^a References: 1. Inserra et al. (2013), 2. Pastorello et al. (2010a), 3. Nicholl et al. (2014), 4. Quimby et al. (2011a), 5. Quimby et al. (2007), 6. Lunnan et al. (2013), 7. Chomiuk et al. (2011), 8. Barbary et al. (2009), 9. McCrum et al. (2014b), 10. Nicholl et al. (2013), 11. McCrum et al. (2014a), 12. Benetti et al. (2014).

* The published magnitude closest in time to the peak of the polynomial fit.

(Chornock et al. 2013; Quimby et al. 2013a, 2014). We also did not include the slowly fading SLSN SN2007bi (Gal-Yam et al. 2009; Young et al. 2010), as it lacks extensive photometric coverage around peak in the blue bands. SN2007bi is not as well sampled in standard filters compared to the excellent coverage of the phenomenologically similar events PTF12dam and PS1-11ap (Nicholl et al. 2013; McCrum et al. 2014a).

In our measurements of the absolute magnitude we considered only the reddening values for interstellar dust in our Galaxy (see Table 1). The SNe of the sample were located in faint, dwarf galaxies and were unlikely to have suffered significant additional extinction. Indeed no absorption due to Na I D lines from gas in the hosts was observed in any spectrum. This does not mean that we can exclude *a priori* possible dust extinction from the host. The assumption that host extinction is uniformly negligible is probably the biggest uncertainty in using SLSN Ic as standard candles. In all cases a standard reddening curve was assumed with $R_V = A_V/E(B-V) = 3.1$. The objects cover a range of redshift between 0.143 and 1.206, hence in the next section we discuss the appropriate corrections needed for redshift effects (K -correction and time dilation) to obtain the absolute rest frame peak magnitudes.

3. DATA ANALYSIS

3.1. Redshift

We assume a cosmology with $H_0 = 72 \text{ km s}^{-1} \text{ Mpc}^{-1}$, $\Omega_m = 0.27$ and $\Omega_\Lambda = 0.73$. All the redshifts used in this paper were evaluated spectroscopically from host galaxy lines (either emission, Mg II absorption or both) with

the exceptions of LSQ12dlf and SN2013dg. For these two, cross-correlation with a library of SLSN spectra was employed, retrieving a typical error on the redshift of ± 0.005 (see Nicholl et al. 2014, for details). In the cases of SN2010gx (Pastorello et al. 2010a; Quimby et al. 2011a), SN2005ap (Quimby et al. 2011a), PS1-10ky (Chomiuk et al. 2011), PTF09cnd (Quimby et al. 2011a), SCP06F6 (Quimby et al. 2011a), PS1-10bzj (Lunnan et al. 2013) and PTF11rks (Quimby et al. 2011b) we retrieved the redshifts by analysing the narrow absorption lines of Mg II doublet $\lambda\lambda 2796, 2803$ and compared to those previously published. For the other three SLSN Ic, we evaluated the redshifts by the identification of host galaxy lines, such as [O II] $\lambda 3727$, [O III] $\lambda\lambda 4959, 5006$, $H\alpha$ and $H\beta$ (cf. with those of Quimby et al. 2010; Drake et al. 2011; Quimby et al. 2011c). In the case of SN2010gx the redshift evaluated by the host galaxy lines (Prieto et al. 2012; Pastorello et al. 2010b,a) is identical to that retrieved through the analysis of Mg II lines (Quimby et al. 2010, 2011a), and there are no cases where there is any measurable difference between the two methods. The two 2007bi-like events (PTF12dam and PS1-11ap) show Mg II lines in absorption. Again, the redshifts determined from this doublet were checked with the emission lines of the host galaxies (as previously done by Nicholl et al. 2013; McCrum et al. 2014a). The typical error on the spectroscopic redshift is ± 0.003 , which corresponds to uncertainties in distance moduli of 0.07, 0.02 and 0.01 at redshifts of $z = 0.1, 0.5$ and 1.0 respectively.

3.2. K -corrections and synthetic photometric bands

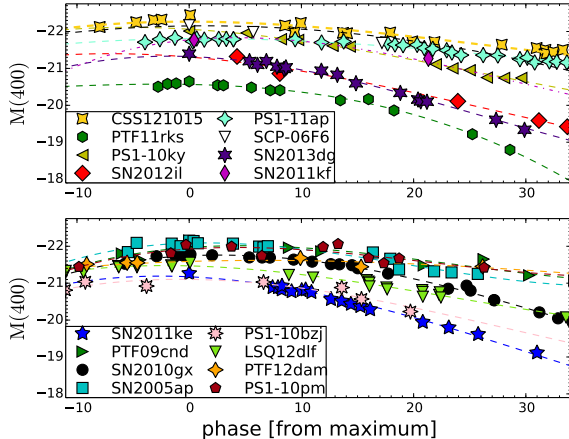


FIG. 2.— Light curves of our SLSN Ic sample listed in Table 1. The absolute magnitudes, $M(400)$ are for the 400nm band after K -correction. Time dilation has been applied to report the phase in restframe days with respect to maximum light. Polynomial fits to the photometry of the sixteen SNe are shown as broken lines. The line fits are all third order polynomials, apart from SN2011kf and SCP06F6 (second order polynomials) and CSS121015 (fourth order polynomial). The objects are split into two panels simply for clarity and illustration purposes.

Photometric and time dependent measurements of objects at significant cosmological redshifts require application of the K -correction and time dilation correction in order to provide meaningful comparative rest frame properties. The K -correction is essential because measurements through a filter in the observer frame detect photons from a different part of the rest frame spectrum than the filter throughput (e.g. Oke & Sandage 1968; Hogg et al. 2002; Blanton & Roweis 2007). This means that an accurate determination for the K -correction requires a flux calibrated spectral energy distribution (SED) which covers a wavelength range large enough for the correction to be calculated. This is ideally done with spectra but multi-color photometric measurements can also be usefully employed to constrain the observed SED. Such K -corrections have been calculated since the early days of using type Ia SNe as distance indicators (e.g. Hamuy et al. 1993; Kim et al. 1996; Nugent et al. 2002) and more recently large libraries of SN Ia spectra have been employed for detailed determination (Hsiao et al. 2007). At low redshift, it is relatively straightforward to calculate corrections to observer frame filter magnitudes such that the rest frame magnitudes are in the same filter band pass. However, at redshifts beyond $z \gtrsim 0.2$, the de-redshifted observed filter function is often closer to another, bluer, standard filter and hence it is more useful to determine K -corrections to a different filter than observed (“cross-filter” K -corrections). For example, at $z = 0.28$ the effective central wavelength of the Pan-STARRS1 r_{P1} filter corresponds to the rest frame g_{P1} filter and hence a K -correction to correct the observed r_{P1} to rest frame g_{P1} is useful (see Tonry et al. 2012, for filter throughput details). When the observed and rest frame filter bands are significantly misaligned, the K -corrections are of course more dependent on the assumed spectral template. The corrections can be computed by using either a theoretical or empirical template spectrum (or SED) at the relevant epoch. Interpolations

of spectra either side of the particular photometric epoch can be used. Nugent et al. (2002) suggested that for SN Ia the dispersion in the cross-filter K -corrections is less than 1% when the interpolated spectra are constrained within ± 4 days of the epoch, whilst Hsiao et al. (2007) showed that with a similar baseline the scatter is probably higher, at 5%.

Typically, K -corrections are calculated to provide magnitudes in rest frame filters that are in a standard system, such as SDSS *ugriz*, or Johnson-Cousins *UBVRI*. In order to make a meaningful comparison of the SLSN Ic absolute magnitudes we need to correct their observed magnitudes to a single filter. While it would be possible to correct to a standard filter in a standard system, it is not clear that this is particularly useful for our purposes. If SLSN Ic are standardizable candles, then their future use is likely to be in redshift regimes beyond those probed by SNe Ia. There is little to be gained by correcting to currently defined rest frame filters since the lack of low redshift SLSN Ic, which have negligible K -corrections, renders the standard filters fairly useless². Instead we choose to define two synthetic rest frame filter band-passes to correct to.

Analysis of the SN rest frame spectra during the first month from the maximum light (Pastorello et al. 2010a; Quimby et al. 2011a; Chomiuk et al. 2011; Inserra et al. 2013), indicates that the region around 4000 Å is continuum dominated and relatively free from strong spectral features that could increase the photometric dispersion from object to object. To determine synthetic magnitudes at this rest-wavelength window, we built the synthetic passband with an effective width of 800 Å and central wavelength at 4000 Å, having steep wings and a flat top (more similar to Sloan than Bessel filters to decrease the errors in the K -correction process). Hereafter we refer to it as the 400 nm band. In a similar way, we defined a second band peaking at 5200 Å with an effective width of 1000 Å, and hereafter refer to it as the 520nm band. Fig. 1 illustrates these synthetic passbands and the rest frame spectral regions lying in them. The choice of these bands was motivated by both the lack of strong spectral features and also by several practical considerations. To maximise the sample size, we required appropriate photometric data that could be K -corrected uniformly to these two bands. If we move the primary restframe band (400nm band) redder (for example close to the standard SDSS r -band which is also relatively featureless) we reduce the complete sample from sixteen objects to eleven. This is due to a lack of photometric data at the appropriate redshifted wavelength region. Furthermore we would not then be able to define a second band (for color tests) since a restframe SDSS i -band (or something similar) would lie beyond the observers z -band, in the near-infrared (NIR). We lack any substantial data for these objects in the NIR. One could consider going the other way and pushing the primary 400nm band bluer, but one must be careful to avoid the strong (and potentially diverse) absorption associated with elements such as Mg II and Si III (see Chomiuk et al. 2011). We did identify a potentially useful region around 3000 Å, which

² This lack of objects known below $z < 0.1$ is simply due to their low volumetric rates.

is the bluest we could consider given the lack of extensive restframe UV spectroscopy. However, using this would reduce our complete sample to just five objects because of a paucity of data in the observer u - or U -band for objects with $z \lesssim 0.3$.

For each SN in question, we calculated K -corrections from a suitable observer frame filter back to the 400nm and 520nm bands. The filters chosen were those that had effective central wavelengths most closely matched to $400(1+z)$ and $520(1+z)$ nm and are listed in Table 1. These are typically g and r -band but the higher redshift objects employ i and z -bands as appropriate. For five of the objects, the available photometry only allowed correction to the bluer 400nm band. When the observed filters used were Bessel, we converted the Vega magnitude into the AB system using the prescription presented in Blanton & Roweis (2007).

We computed K -corrections with our own *python* based code which we term SuperNova Algorithm for K -correction Evaluation (SNAKE; a full description will be published in Inserra et al. in preparation along with a code release). We calculated K -corrections for each photometric point available in the literature for each SN using an observed spectrum at the same, or similar epoch within ± 4 days from the photometry. For photometric epochs for which no spectra were available, we determined a SED using the multi-color photometric measurements available. If all colors were not available at the specified epoch, we allowed a window of ± 2 days to select the photometric measurements. If both spectra and photometry were absent we used our library of spectra that includes 78 spectra from seventeen SLSN Ic (including 2007bi-like SLSN). In Table 2 we report the K -corrections at key epochs along with the method used to evaluate them (see Appendix B for error treatment and differences between the three methods). A time dilation correction of $(1+z)$ was applied to all epochs with respect to the peak magnitude which was defined as $phase = 0$. The absolute magnitudes were then calculated from

$$m_f = M(400) + \mu + K_{f \rightarrow 400} + A_f, \quad (1)$$

where m_f is the AB magnitude in the observed filter f , μ is the distance modulus calculated from the luminosity distance for our adopted cosmology of $H_0 = 72 \text{ km s}^{-1} \text{ Mpc}^{-1}$, $\Omega_m = 0.27$ and $\Omega_\Lambda = 0.73$; A_f is the Galactic extinction in the observed filter; and $K_{f \rightarrow 400}$ is the K -correction from the observed filter in Table 1 to the synthetic 400nm bandpass. The $M(400)$ lightcurves and the $M(400) - M(520)$ color evolution curves of all the SNe after these K -corrections are shown in Fig. 2 and Fig. 3. The errors on the absolute magnitudes are estimated by propagating the errors of the four terms in Equation 1, including an estimate of the uncertainty in the K -correction (details are in Appendix B).

3.3. Absolute peak magnitudes and light-curve interpolation

Most of the sample of sixteen SNe had enough data points around peak to secure a confident estimate of both the value and epoch of the peak magnitude in the 400nm band. However not all SNe had specific measurements exactly at the four key epochs we identified as having useful diagnostic power. These epochs are at peak (de-

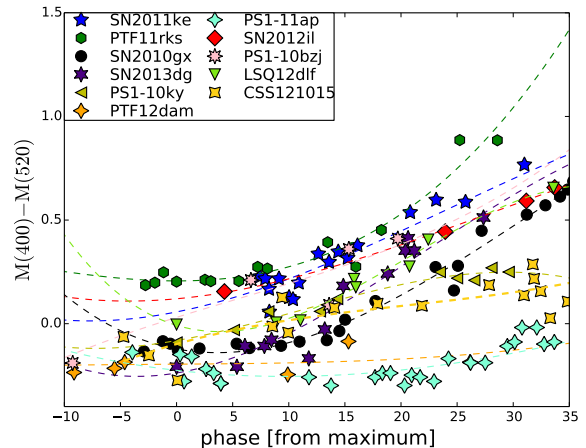


FIG. 3.— Color evolution as measured from the $M(400) - M(520)$ color index vs restframe phase in days. The reference phase of zero days is the epoch of maximum in the 400nm band. K -corrections and time dilation have been applied. Polynomial fits to the color evolution are shown. The color of SN 2012il close to peak was evaluated using spectra (see Appendix A for details). All line fits represent third order polynomials (dashed lines), apart from that for PS1-10ky which was fitted with a fourth order polynomial (dotted line).

finned as 0 days) and after +10, +20 and +30 days (rest frame). We employed a consistent method of polynomial fits to the $M(400)$ data points to allow estimates of the magnitudes at these epochs. We found polynomials of order from 2 to 4 were sufficient and the results of these fits are plotted over the data points in Fig. 2. Similarly, polynomial fits to the $M(400) - M(520)$ color curves were calculated (either third or fourth order) and are plotted in Fig. 3. The specific details for each light-curve fit are given in the Appendix A. The fits displayed in Figures 2 & 3 and the magnitudes reported in Table 1 are those from the values of the polynomial interpolation at the specific epochs of peak, +10d, +20d and +30d, unless otherwise noted (see Appendix A for details on each object).

The peak absolute magnitudes of the pure sample (see Section 2) give a mean of $M(400) = -21.64 \pm 0.46$ where the latter number is the standard deviation of the sample³. If the two slowly declining, 2007bi-like SLSN are included then the extended sample mean and standard deviation are not significantly changed $M(400) = -21.65 \pm 0.43$. We also obtain a similar scatter of $M(400) = -21.70 \pm 0.46$ in the complete case. This raw, and uncorrected range is quite encouraging since the bulk of normal (often historically known as “Branch” normal) type Ia SN originally had uncorrected peak magnitudes with scatters of ± 0.8 , 0.6 and 0.5 in BVI respectively (Phillips 1993). The sample of Prieto et al. (2006) was a factor of ten larger and showed slightly higher values for the raw standard deviation ± 0.9 , 0.7, 0.6, 0.6 in $BVRI$ respectively.

In Figure 4 the histograms of the absolute peak magnitudes of our samples are shown. The numbers in each bin are understandably small, but the distribution is consistent with being approximately gaussian. Considering

³ To be clear, we are assuming that these thirteen objects are a sample of a larger population, hence the sample standard deviation is calculated using $(n - 1)$ as a denominator.

TABLE 2
CALCULATED K -CORRECTIONS FOR THE SAMPLE OF SLSN.

SN	z	$K_{f \rightarrow 400}^{\text{peak}}$	$K_{f \rightarrow 400}^{10}$	$K_{f \rightarrow 400}^{20}$	$K_{f \rightarrow 400}^{30}$	$K_{f \rightarrow 520}^{\text{peak}}$	$K_{f \rightarrow 520}^{30}$
SLSN Ic (2005ap-like)							
SN2011ke	0.143	-0.18 (P)	-0.17 (S)	-0.22 (S)	-0.24 (P)	-0.11 (S)	-0.16 (S)
SN2012il	0.175	-0.18 (L)	-0.18 (S)	-0.23 (L)	-0.25 (P)	-0.09 (L)	-0.15 (P)
PTF11rks	0.190	-0.19 (S)	-0.17 (S)	-0.16 (S)	-0.17 (P)	-0.19 (S)	-0.19 (P)
SN2010gx	0.230	-0.23 (S)	-0.18 (S)	-0.18 (S)	-0.07 (S)	-0.23 (S)	-0.20 (S)
SN2011kf	0.245	-0.13 (L)	-0.10 (L)	-0.08 (S)	-0.08 (S)	-	-
LSQ12dlf	0.255	-0.17 (S)	-0.15 (S)	-0.29 (S)	-0.38 (S)	-0.28 (S)	-0.20 (S)
PTF09cnd	0.258	-0.34 (S)	-0.29 (L)	-0.29 (L)	-0.16 (L)	-	-
SN2013dg	0.265	-0.30 (P)	-0.25 (S)	-0.40 (S)	-0.47 (S)	-0.45 (S)	-0.40 (S)
SN2005ap	0.283	-0.33 (S)	-0.57 (L)	-0.60 (L)	-	-	-
PS1-10bjz	0.650	-0.58 (P)	-0.57 (S)	-0.46 (S)	-0.48 (L)	-0.37 (P)	-0.53 (L)
PS1-10ky	0.956	-0.73 (S)	-0.75 (P)	-0.76 (P)	-0.68 (S)	-0.65 (P)	-0.59 (P)
SCP-06F6	1.189	-1.35 (L)	-1.45 (L)	-1.51 (L)	-1.56 (L)	-	-
PS1-10pm	1.206	-0.84 (P)	-0.96 (P)	-1.04 (P)	-	-	-
SLSN Ic (2007bi-like)							
PTF12dam	0.107	-0.07 (S)	-0.02 (S)	+0.04 (S)	+0.04 (S)	-0.03 (S)	+0.01 (S)
PS1-11ap	0.524	-0.45 (S)	-0.42 (S)	-0.43 (P)	-0.47 (P)	-0.47 (S)	-0.53 (P)
SLSN II							
CSS121015	0.287	-0.37 (S)	-0.36 (S)	-0.35 (S)	-0.32 (P)	-0.40 (S)	-0.22 (P)

NOTE. — (S) denotes that a spectrum of the same object has been used to evaluate the K -correction. (P) indicates that the multi-color photometry of the object was used, while (L) means that we used our library of spectra.

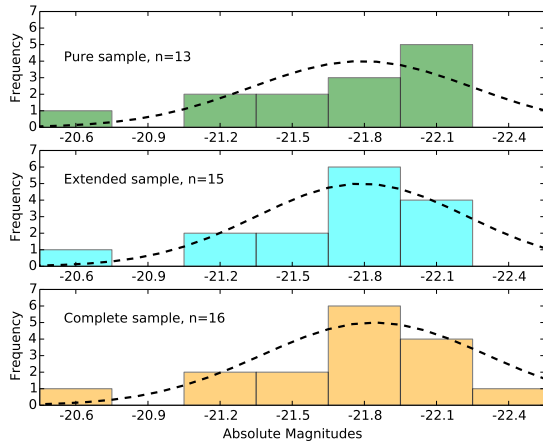


FIG. 4.— Histograms of the raw (uncorrected) absolute peak magnitudes, $M(400)$, for the three samples defined in Section 2. The dashed lines are least squares, best fit Gaussians. Assuming confidence limits for small number events from Gehrels (1986), the Gaussian fits all comfortably fall within the 1σ errors of the frequencies.

the statistical errors on the frequency in each bin (see small number confidence limits in Gehrels 1986) we find no evidence for a non-Gaussian distribution of peak magnitudes.

4. THE PEAK MAGNITUDE - DECLINE RATE RELATION

The now famous Phillips relation for type Ia SNe links the rate of decline of a B -band SN Ia light-curve to the absolute B magnitude at peak (Phillips 1993). The original paper by Phillips brought the intrinsic scatter in SNe Ia peak magnitudes down from the raw ± 0.8 in B to ± 0.36 , and Prieto et al.’s larger sample produced a scatter of ± 0.2 . To determine if SLSN are standard-

izable in a similar way and if the raw scatter of ± 0.46 mag can be improved upon, we correlated the absolute peak magnitude, $M(400)$, with the amount that the light curve fades from the maximum at three defined periods following peak light.

We chose the timescales of 10, 20 and 30 days post maximum and refer to the difference between peak magnitude at these epochs as $\Delta M_{10}(400)$, $\Delta M_{20}(400)$ and $\Delta M_{30}(400)$ respectively. It is not possible to meaningfully test the extension of the time baseline beyond 30 days as the sample size would reduce considerably due to lack of data at these epochs. The magnitudes of each SN at these epochs were estimated from the polynomial fits to the light-curve points as described in Section 3.3 with the only exception of the peak magnitude of CSS121015 (cfr. Appendix A). In Fig. 5 we plot the relation between $M(400)$ and the decline rates at 10, 20 and 30 days. The plots indicate that the peak magnitude of SLSN Ic does appear to be correlated with decline rate in the same sense as for the Phillips relation for SNe Ia. The brighter the peak magnitude (in the rest frame 400nm band) the more slowly they fade. The question then becomes : is this quantitatively useful to reduce the intrinsic scatter in the uncorrected peak magnitudes below the **raw scatter of ± 0.46 mag** ?

The least square fits to the data points are shown and their parameters are given in Table 3. These suggest that the scatter can indeed be improved upon to between **0.25 and 0.33 depending** on the epoch at which the decline rate is applied and which object sample to include. The most promising relation that we find is that **for $\Delta M_{30}(400)$, which reduces the scatter from ± 0.46 mag to ± 0.25 mag using** the pure sample of SLSN Ic. The correlation at 20 days after peak, $\Delta M_{20}(400)$, is **similar to that at 30 days**. Although the rms scatter is formally larger, the difference is not particu-

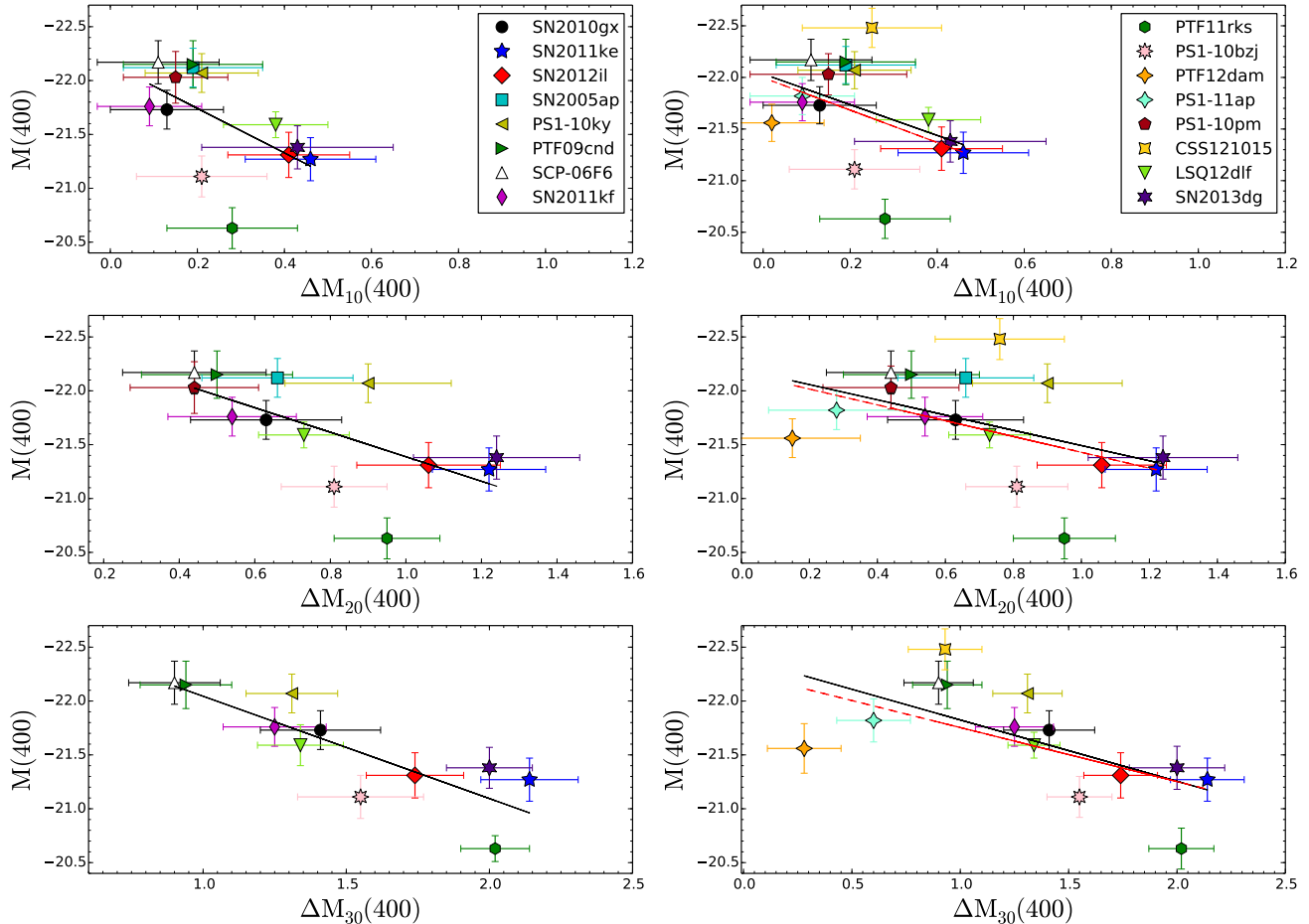


FIG. 5.— The peak magnitude - decline rate relation. The absolute peak magnitude in the 400nm band, $M(400)$, is plotted versus $\Delta M_{10}(400)$, $\Delta M_{20}(400)$ and $\Delta M_{30}(400)$. The latter three values are measures of the light-curve decline (in magnitudes) during the first 10, 20 and 30 days after maximum. The left-hand column of plots shows only the 2005ap-like events (pure sample) and the right-hand column shows all SLSN. The dashed-red line is the fit of the extended sample, while the black of the complete sample (see Section 2 for the sample definitions). The SN magnitudes and the corresponding $\Delta M_{\text{day}}(400)$ are reported in Table 1, while the parameters of the linear regression fits (black line) are listed in Table 3.

larly significant (0.03 to 0.09). **Indeed, the Spearman rank-order correlation coefficient for the $\Delta M_{30}(400)$ rate is 0.90 while the Pearson’s r test gives a result of 0.84** and are also reported in full for each fit in Table 3.

The Pearson correlation coefficient for the $\Delta M_{30}(400)$ is higher than the $\Delta M_{20}(400)$, and is usually the most commonly employed statistic. It measures the strength of the linear relationship between normally distributed variables. When the variables are not normally scattered, or the relationship between the variables is not linear, it may be more appropriate to use the Spearman rank correlation method. Indeed, the Spearman rank correlation method makes no assumptions about the distribution of the data.

For the extended sample the scatter increases to ± 0.33 mag (± 0.36 mag at 20d) and the Spearman correlation coefficient and Pearson’s r are significantly reduced. This simple statistical result and visual inspection of the correlation plots in Fig. 5 would suggest that the 2007bi-like, slowly fading SLSN differ from the rest of the SLSN Ic. If they are included in the total sample, then it may result in distribution with an asymmetric tail and non-

negligible kurtosis. In this case we should be careful in assuming a normal distribution for the parameters of all SLSN. It is not yet clear if PTF12dam, PS1-11ap and SN007bi are physically different explosions to the rest of the SLSN Ic, nor is it clear if there is a continuum between the fast and slowly declining events. The next slowest SLSN Ic are PS1-10pm and SCP-06F6, which do sit comfortably on all the straight line fits.

If we would consider the complete sample then the scatter would **increase to ± 0.36 mag (or ± 0.41 mag at 20d)**, with a marginal decrease in the statistical correlation coefficients. We would highlight that we are presenting the results grouped in these three ways simply due to the fact that the observational characteristics of the three groups are quite easily distinguished in this low-moderate redshift sample. However, if one were working at high redshift then the subtleties of the different samples and observational classes may be difficult to distinguish.

In Section 3.2 we described how the wavelength window for the synthetic 400nm photometric band was chosen. The spectra of all objects in this region are con-

TABLE 3
FIT PARAMETERS AND STATISTICAL RESULTS OF OUR PURE, EXTENDED AND COMPLETE SAMPLE

Days	N (objects)	a	b	σ (mag)	Spearman	Pearson
$\Delta M_{\text{day}}(400)$ pure sample						
10	13	2.06 (1.17)	-22.15 (0.29)	0.38	0.65	0.56
20	13	1.19 (0.47)	-22.53 (0.37)	0.34	0.73	0.66
30	11	0.95 (0.23)	-22.99 (0.35)	0.25	0.90	0.84
$\Delta M(400 - 520)$ pure sample						
30	8	2.02 (0.42)	-22.64 (0.26)	0.19	0.71	0.88
$\Delta M_{\text{day}}(400)$ extended sample						
10	15	1.57 (0.99)	-22.00 (0.22)	0.38	0.51	0.49
20	15	0.73 (0.37)	-22.16 (0.26)	0.36	0.58	0.54
30	13	0.50 (0.20)	-22.26 (0.27)	0.33	0.75	0.64
$\Delta M(400 - 520)$ extended sample						
30	10	1.09 (0.45)	-22.00 (0.23)	0.26	0.70	0.74
$\Delta M_{\text{day}}(400)$ complete sample						
10	16	1.49 (1.10)	-22.03 (0.25)	0.42	0.42	0.42
20	16	0.71 (0.42)	-22.20 (0.30)	0.41	0.51	0.47
30	14	0.57 (0.22)	-22.39 (0.28)	0.36	0.74	0.64
$\Delta M(400 - 520)$ complete sample						
30	11	1.34 (0.42)	-22.19 (0.20)	0.31	0.71	0.75

NOTE. — Least squares fits for an unweighted linear fit of the form $M_{\text{max}}(400) = a\Delta M_{\text{day}}(400) + b$ with uncertainties in parentheses. The σ is the standard deviation of this fit. The last column gives the Spearman rank-order correlation coefficient and the Pearson correlation coefficient r . As the errors on each value of $M(400)$ are fairly similar, a weighted calculation is not significantly different. For completeness, we have reported the fit values obtained excluding CSS121015. Although SN2005ap and PS1-10pm are left out of the 30 day decline calculations as they do not have enough data.

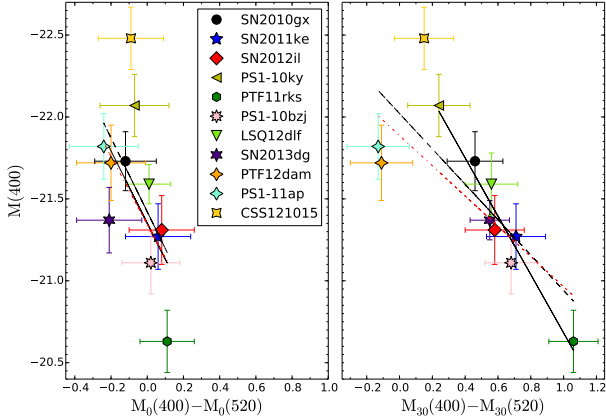


FIG. 6.— The peak magnitude - color evolution relation. This plot illustrates the apparent dependency of peak magnitude on the color and color evolution rate. The left panel plots the $M(400)$ peak magnitude versus the color at peak brightness. The right panel plots the same $M(400)$ at peak versus the color at +30 days (rest frame). The black line fit refers only to the pure sample (2005ap-like objects), the red dot-dashed line fits the extended sample (which includes the 2007bi-like objects) while the black dashed line fits the complete sample.

tinuum dominated and relatively similar in slope and spectral features. Nevertheless there are some absorption features present and the O II lines are typically the strongest features at $\lambda \geq 4200 \text{ \AA}$. These features are

on the red edge of our window and show noticeable absorption before maximum light (Pastorello et al. 2010a; Quimby et al. 2011a; Chomiuk et al. 2011). At peak brightness, the O II absorption at $\sim 4000 \text{ \AA}$ is relatively shallow and remains weak in the following 20 days (Pastorello et al. 2010a; Inserra et al. 2013). At 30 days past maximum, absorption due to Mg II and Fe II become noticeably stronger than the O II lines. In our spectroscopic analysis we found two objects, namely PTF11rks and PS1-10bjz, that seem to show noticeable differences in their spectroscopic evolution with respect to the bulk of SLSN Ic. The Mg II and Fe II lines between 3000 \AA and 6000 \AA , and Si II $\lambda 6355$ are stronger in these two objects than the rest of the sample. In the first two weeks after peak, PTF11rks shows absorption line equivalent widths which are a factor of 4 greater than the bulk of the sample ($EW_{\text{PTF11rks}} = 4 \pm 1.5 EW_{\text{SLSN Ic}}$). The strengths of these features are noticeable in Fig.1. The PS1-10bjz spectra after maximum light also show a qualitatively similar line intensity evolution, although not as pronounced as PTF11rks. We note that the lower S/N of the spectra of PS1-10bjz prevent as detailed and quantitative measurements as were possible for PTF11rks, but both appear to evolve on faster timescales than the rest of the SLSN Ic. For completeness, we tested the $\Delta M_{30}(400)$ relation *excluding* PTF11rks and PS1-10bjz from the pure sample. We found that the scatter was substantially reduced to ± 0.14 and we retrieved a Spear-

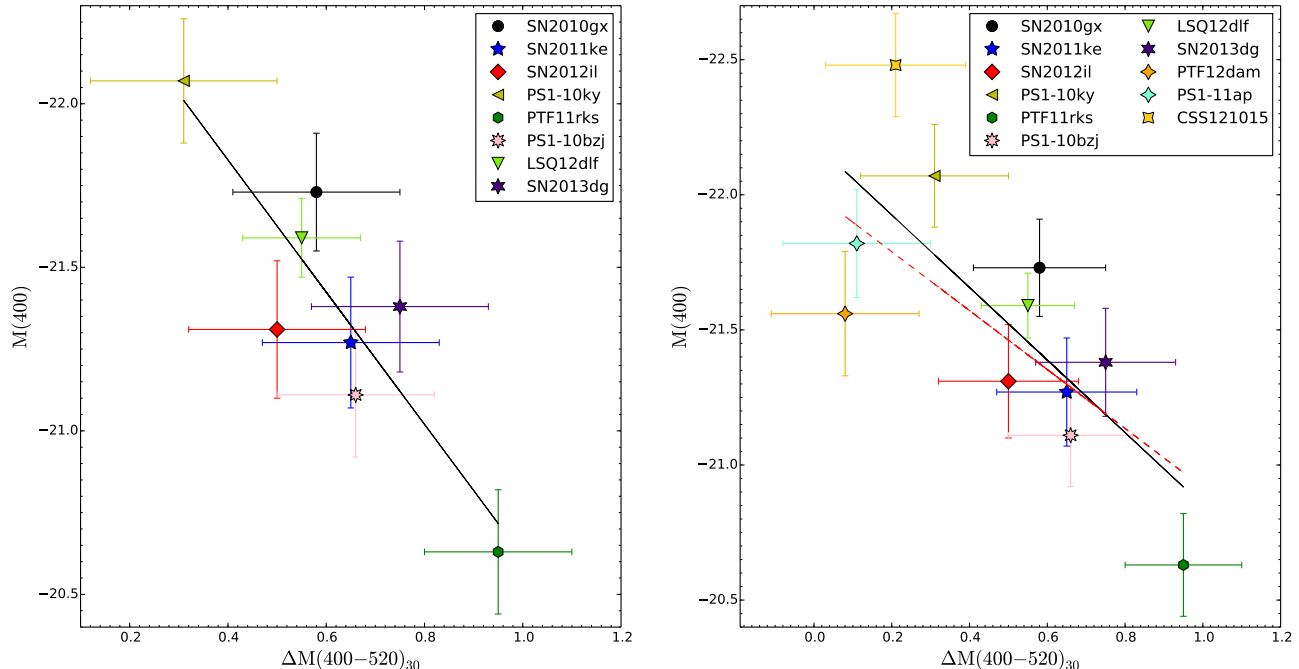


FIG. 7.— The peak magnitude - color evolution relation. Absolute peak magnitudes in the 400nm band, $M(400)$, versus the color change from peak to +30 days (rest frame). We define $\Delta M(400 - 520)_{30} = (M_0(400) - M_0(520)) - (M_{30}(400) - M_{30}(520))$. The bands at 400nm and 520nm are defined in Section 3.2, and the values for $\Delta M(400 - 520)_{30}$ values are reported in Table 1. *Left*: a plot of eight of the pure sample which have the necessary bands covered in the observer frame to calculate this color term. *Right*: eleven objects of the complete sample which have the necessary data. The black lines are least squares straight line fits to all data in each plot. The red dotted line leaves out CSS121015. The parameters of these line fits are listed in Table 3.

man rank-order correlation coefficient of **0.95 while the Pearson’s r test is 0.91**. The statistical results are slightly better than those obtained with all objects of the pure sample. This might suggest that these two SNe appear to have spectroscopic and photometric differences compared to the bulk of the population. However, identifying these potential outliers in the distribution is too subtle to be achieved without a well-sampled time series of high signal-to-noise optical and near-UV spectra. Such identification would be difficult for high redshift objects.

5. THE PEAK MAGNITUDE - COLOR EVOLUTION RELATION

In Section 3.2 we defined two synthetic photometric bands centred on 400nm and 520nm as regions of the rest frame spectra which were mostly devoid of strong SN absorption features and were, on the whole, continuum dominated. The rest frame color evolution of the objects, based on these two photometric indices, is plotted in Fig. 3. This immediately illustrates a large diversity in color evolution which is visible at peak and increases substantially during the first 30 days. This is further illustrated in Fig. 6, where we plot the absolute peak magnitude $M(400)$ against the color term $M(400) - M(520)$ at peak and after 30 days. The peak absolute magnitude $M(400)$ appears to be color dependent, in the sense that objects which are fainter at peak are redder. If it were a real correlation, one would immediately consider internal host galaxy extinction as a possible explanation and we discuss this at the end of this section.

A much more striking trend is that the fainter objects tend to become redder faster. In other words, the rate of color change appears to be correlated with peak mag-

nitude. This strong dependency is displayed in Figure 7, where we show that the peak absolute magnitude is correlated quite tightly with the *rate* of color evolution. In the pure sample, we are reduced to only eight objects due the requirement for data covering the rest frame 400nm and 520nm bands at both peak and at +30 days. This could potentially bias the result toward a positive result and artificially reduce the scatter around the straight line fit. However the rms scatter around the linear least squares fit is reduced to **0.19 mag** for the eight objects of the pure sample. The two statistical correlation tests result in **0.71 for the Spearman coefficient and 0.88 for the r Pearson’s coefficient**. For the ten objects of the extended sample the residual rms is **still quite low at 0.26 mag**. It increases to 0.31 mag for the complete sample, when CSS121015 is included. From Figs. 6 and 7 it is clear that PTF12dam and PS1-11ap are systematically bluer than the rest of the SLSN Ic both at peak and at +30 days, and CSS121015 also sits significantly above the best linear fit.

For completeness, we also checked the correlation over the 20 day evolution timescale and found a poorer correlation. **For $\Delta M(400 - 520)_{20}$ we found an rms of 0.30 mag (0.29 for the extended sample) and lower statistical coefficients than for the $\Delta M(400 - 520)_{30}$ (0.67 for the Spearman coefficient and 0.67 for the r Pearson’s coefficient)**. Hence the 30 day color rate evolution seems significantly better. Although the numbers are low, this peak magnitude - color evolution relation appears to be quite promising as a method of standardizing the magnitudes of SLSN. The rms scatter is surprisingly low, even with the inclusion of the most outlying three objects in the complete sample. The very

tight correlation for the eight SLSN Ic of the pure sample makes it imperative that this relationship is tested with a larger sample.

The major uncertainty is extinction within the host galaxies. We have made no correction for internal dust extinction and it is difficult to quantitatively measure reddening from either the colors, spectrum slope or interstellar medium lines in this small sample (indeed we do not detect ISM NaI lines from the ISM in the host galaxies for any SLSN). One might be concerned that the left panel in Fig. 7 was a reddening effect if we simply observed that the fainter SLSN were redder at peak. An argument against it being extinction is that both PTF11rks and PS1-10bzj have qualitatively different evolution in their spectral features (deeper Mg II, Fe II and Si II absorption) than the rest of the pure sample. This suggests cooler photospheric temperatures rather than an extinction effect (see discussion in Section 4). The brightest object (CSS121015) is also spectroscopically different in that H α was detected and it may well be physically different to the others. Constant extinction values might explain the connection between color and luminosity, but they cannot easily account for the observed color evolution in the light curves. The distinctive time evolution of the $M(400) - M(520)$ color could, in principle, be due to time-variable internal dust extinction. However, to our knowledge, such time variability has not been observed before toward any supernova. Time variable interstellar and circumstellar medium absorption lines have been observed toward SNe Ia (Patat et al. 2007), but these have not been linked with variable extinction toward the SN photosphere. In the future, a more sophisticated approach would be to combine fits for decline and color evolution into one standardization procedure as has been successfully done for SNe Ia e.g. methods like SALT2 (Guy et al. 2007). Or to use Bayesian methods to simultaneously model dust and color effects as in Mandel et al. (2009, 2011). Additionally we plan to look for extinction signatures by searching for objects with identical photospheric spectra but which have different colors and continuum slopes. This would ideally include near infrared photometric fluxes to anchor the SED fits securely. Both of these approaches require a more extensive data set than we have presented here, which should be possible given the ongoing low redshift surveys such as PESSTO and La Silla QUEST (Baltay et al. 2013, Smartt et al. in prep.), CRTS (Drake et al. 2009) and iPTF (Cao et al. 2013).

5.1. A control test : application to Type Ib/c

As a sanity check we investigated if the relations we appear to have discovered for SLSN Ic also manifest themselves in the normal type Ib/c SN population and hence if we are recovering characteristics which are commonly displayed in more normal hydrogen poor stellar explosions. We performed the same analysis with a sample of well observed stripped-envelope SN (type Ic, Ib, IIb), with the only difference from the SLSN Ic analysis being the choice of the reference bands. We chose the Johnson B -band with central peak wavelength at 4448 Å and Johnson V -band 5505 Å, due to the excellent sampling of the low-redshift observed SN Ib/c in this standard wavebands (which were not in need of any K -correction). As shown in Figure 8 there is no relation between the

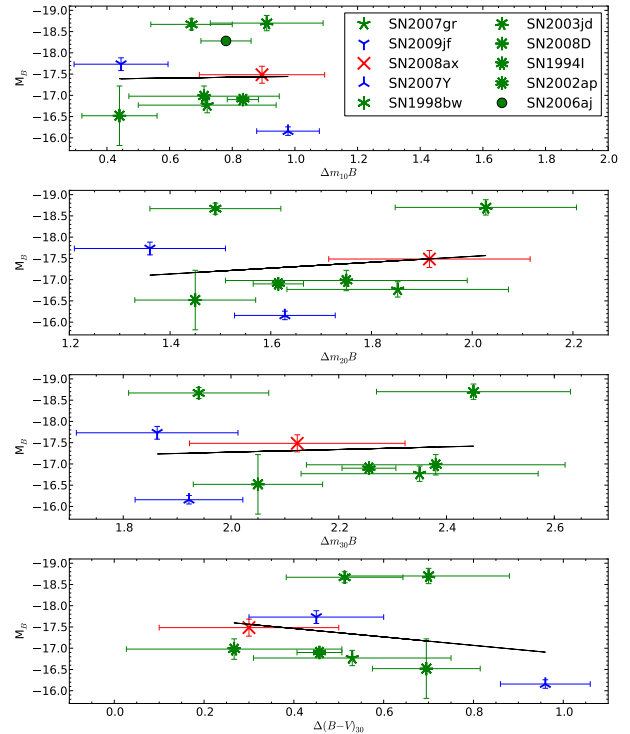


FIG. 8.— The peak magnitude - decline relation and the peak magnitude - color evolution relation for ten stripped envelope CCSN. Absolute magnitudes in the B -band are plotted versus $\Delta m_{10}(B)$, $\Delta m_{20}(B)$ and $\Delta m_{30}(B)$ analogous to the SLSN sample in Fig. 5. The $\Delta(B - V)_{30}$, measures the color evolution in $B - V$ over 30 days. The data sources are as follows : the type Ic SN 2007gr (Valenti et al. 2008b; Hunter et al. 2009), 1998bw (Galama et al. 1998; McKenzie & Schaefer 1999; Sollerman et al. 2000; Patat et al. 2001), 2003jd (Valenti et al. 2008a), 2008D (Mazzali et al. 2008; Soderberg et al. 2008; Modjaz et al. 2009), 1994I (Richmond et al. 1996), 2002ap (Pandey et al. 2003; Foley et al. 2003; Yoshii et al. 2003; Tomita et al. 2006) and 2006aj (Campana et al. 2006; Cobb et al. 2006; Mirabal et al. 2006; Pian et al. 2006; Sollerman et al. 2006); the type Ib SN 2007Y (Stritzinger et al. 2009), 2009jf (Valenti et al. 2011) and the type IIb SN 2008ax (Pastorello et al. 2008).

peak magnitudes and the decline rates at 10, 20 and 30 days or with the color evolution. As expected, we find a large scatter of peak magnitudes and no obvious correlations which mimic the findings for the SLSN. The mean and raw scatter in the M_B values for type Ibc SN are -17.42 ± 0.90 , and this is not improved when any linear fits are applied.

6. HUBBLE DIAGRAM AND RESIDUALS

If we assume that SLSN Ic can be used as standardizable candles and then apply the ΔM_{30} decline relation (calibrated with 11 objects) and the peak magnitude - color evolution relation (with the 8 objects reported in Sect. 5), then we can use these as a preliminary test to check if they fall in a reasonable region of the Hubble diagram, as shown in Figure 9. The small number of objects and lack of a low redshift anchor prevents any detailed discrimination between cosmology models but consistency checks of the relative distances for a cosmology with $\Omega_\Lambda = 0$ is possible.

We evaluated the distance moduli with the simple formalism $\mu = m - M + \alpha \Delta M$, where ΔM refers to the standardization relation used and α is a free parameter.

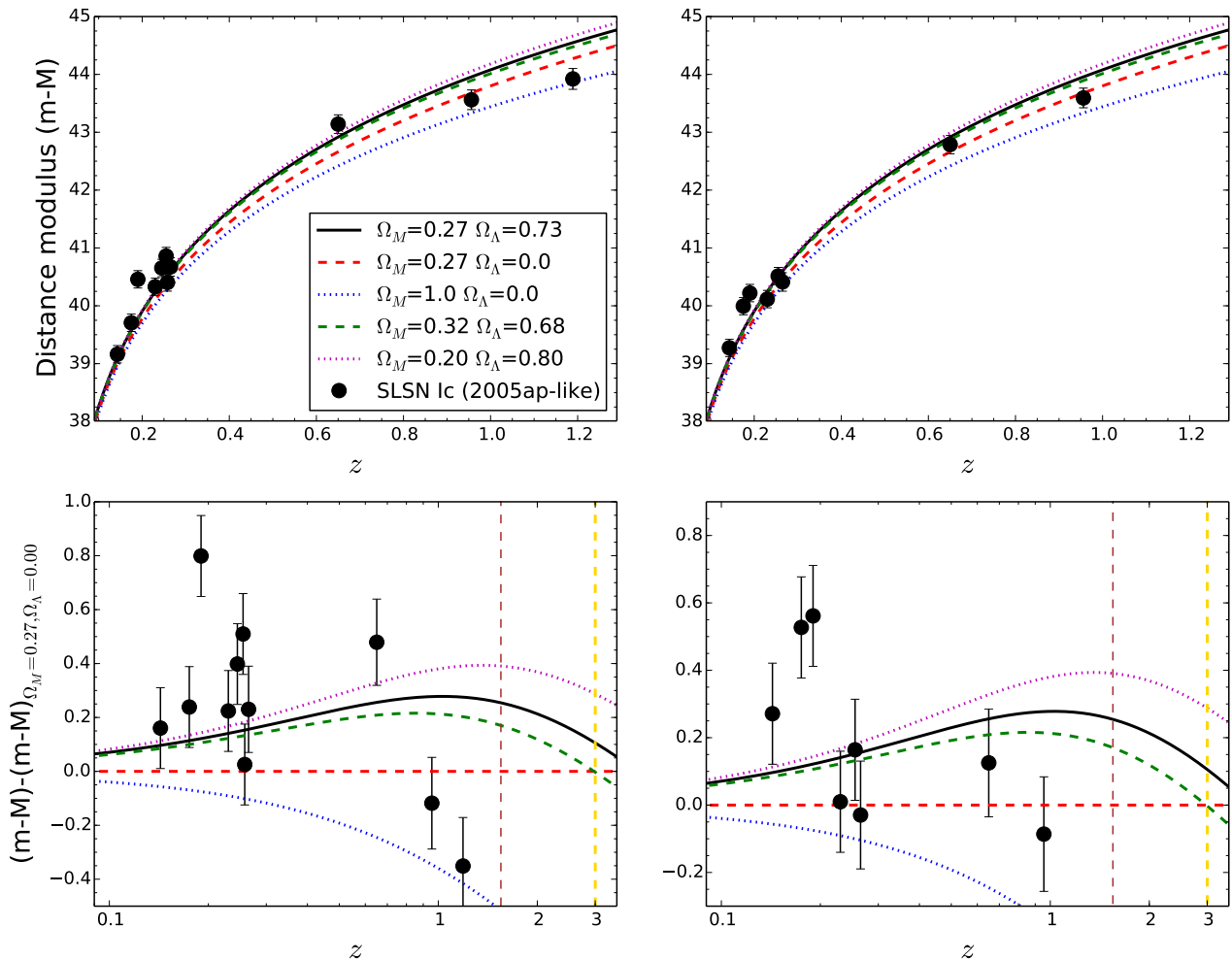


FIG. 9.— Hubble diagrams for SLSN Ic. Different cosmologies are plotted in comparison with that chosen (solid black line) to measure the distance moduli of the sample presented. *Left panels:* The distance moduli measured using the ΔM_{30} decline relation *Right panels:* The distance moduli measured using the peak magnitude - color decline relation. The lower panels show the residuals of the distances relative to a $\Omega_M = 0.27, \Omega_\Lambda = 0$ Universe. The brown, dashed vertical line represents the SNe Ia upper limit with the current generation of telescopes (ground and space), whereas the gold, dashed line represents an approximate limit for discovery and monitoring of SLSN Ic with the current generation of telescopes.

This parameter α is allowed to vary and to minimise the χ^2 between the fit to the distance moduli and those for different cosmologies. Because of our statistically limited dataset, we can only determine if the data are consistent with a $H_0 = 72, \Omega_M = 0.27, \Omega_\Lambda = 0.73$ universe. We found a satisfactory fit, and the lowest χ^2 for this concordant cosmology model. If we attempt a fit with $\Omega_\Lambda = 0, \Omega_M = 1$, then we get a χ^2 which is a factor of 10 worse, and an unsatisfactory Hubble diagram fit. This simply illustrates that the relative distances to these SLSN are not compatible with a cosmological model with $\Omega_\Lambda = 0$, but we do not have enough statistics to test it any further.

The results of the best fit are displayed in Figure 9. It also indicates that distance indicators in the range of $0.6 \lesssim z \lesssim 3$, where SLSN Ic are already discoverable with the current generation of telescopes, may give us some leverage on Ω_M since the difference between $\Omega_M = 0.20$ and 0.32 is ~ 0.3 mag which would be well within the reach of a sample of 10 – 20 SLSN Ic in the redshift

range $z = 2 - 3$. SLSN will probably not achieve a competitive precision to **rival Ω_Λ measurements** from either Baryon Acoustic Oscillations (Eisenstein et al. 2005; Percival et al. 2010) or Cosmic Microwave Background experiments (Dunkley et al. 2009; Komatsu et al. 2011) as already noted by Suzuki et al. (2012). However since SLSN are the only current alternative to SN Ia for estimating radial distances at high redshift, it is worth exploring if they can constrain the time-varying nature of $w(z)$, the dark energy equation-of-state parameter. The study of SLSN at high- z is also a promising avenue to explore the nature of the explosions and sources of luminosity and to investigate if there are changes in their properties with epoch and environment (see Appendix C).

In the future, we plan to tie down the calibrations for these potential standardizable candles in the lower redshift regime of $0.1 < z < 0.3$ simply by increasing the number of objects discovered and monitored in detail. Their cosmological usefulness may stem primarily from their ability to be discovered and studied in the redshift

regime beyond that for SNe Ia, which is currently around $z = 1.55$ (Rodney et al. 2012).

7. FUTURE USE OF SLSN AS HIGH REDSHIFT DISTANCE PROBES

If our results are confirmed with a larger sample then these SLSN show potential as new cosmological probes stretching well into the epoch of deceleration. At $z \geq 1$, the synthetic passbands at 400 and 520 nm move into the near-infrared. We primarily chose the central wavelength and width of these rest frame bands due to the lack of strong features in the SLSN Ic spectra (see Section 3.2) but we also considered the location and width of the redshifted passbands in the observer frame at $1 \lesssim z \lesssim 4$. In Figure 10 we show the two bands redshifted at $z = 1, 2, 3, 4$. The 400nm band covers a similar wavelength region to the Sloan *i*-band, the NIR *J*-band, *H*-band and partially the *K* band, respectively. Observations in these bands would mitigate the dependence of the cross-filter *K*-correction on the spectral template used. Similarly, the 520nm band would be reasonably well covered at $z = 1, 2, 3$ by the standard filter bands *Y*, *H* and *K*, respectively. No standard ground-based filter band is found to match the 520nm band at $z = 4$ due to atmospheric absorption from $\sim 2.5\mu\text{m}$ to $\sim 3.5\mu\text{m}$. As an example, typical average magnitudes of SLSN in the rest frame 400 nm band would correspond to $J \sim 23.0$, $H \sim 23.8$ and $K \sim 24.3$ mag at $z = 2, 3, 4$ respectively. The exposure times with the VLT and HAWK-I are between 2-4hrs to reach a signal-to-noise of 10 for these magnitudes. While the Wide Field Camera 3 (WFC3) on the Hubble Space Telescope can only get to *J* and *H* equivalent wavelengths (F110W and F160W), one can reach improved photometric precision ($S/N \simeq 50$) in manageable exposure times of between 300s to 3000s on source. While these are feasible as dedicated follow-up projects, neither HAWK-I nor WFC3 are appropriate survey instruments to find them in large numbers due to their limited field size (tens of square arc minutes). A more appropriate search engine is a planned survey such as ‘‘SUDSS’’ (Survey Using Decam for Super-luminous Supernovae) using the Dark Energy Camera on the CTIO Blanco 4m telescope. This project has a goal of discovering 200 SLSN out to $z \simeq 4$ over 3 years by imaging approximately 24 square degrees (in *griz*) to $i \simeq 25$ every 14 days. The planned Subaru/Hyper Suprime-Cam deep survey will also target these high redshift objects, with encouraging numbers estimated by Tanaka et al. (2012). The NIR imaging follow-up would be required to reach the rest frame 400nm and 520nm bands and exploit our proposed standardizing of the peak magnitudes. Identification of the redshifts would not require spectra in the NIR, but could be done in the optical observer frame (rest frame UV wavelengths between 1200-2500Å) where the SLSN are predicted to peak around $i = 23.5$ at $z \simeq 3$.

Despite their enormous luminosity and potential for standardizing the peak magnitudes, two practical difficulties remain. The first is that we have only eight to thirteen SLSN (depending on sample selection) having sufficient multi-color data at the epochs and filters required, thus increasing the sample is mandatory. The second is their low volumetric rate of cosmic production. A rough estimate of their rate in the local universe was

provided by Quimby et al. (2013b), who reported a rate of 32_{-26}^{+77} events $h_{71}^3 \text{ Gpc}^{-3} \text{ year}^{-1}$ at a weighted redshift $\bar{z} = 0.17$ although was based on only one detected object (SN2005ap) in the Texas Supernova Search (TSS). While the number is uncertain, the TSS and PTF (Quimby et al. 2011a) do demonstrate that the SLSN rate in the local universe is low compared to that of SN Ia (0.01%). McCrum et al. (2014b) has estimated a rate of $6_{-2.4}^{+3.6} \times 10^{-5}$ and $1_{-0.8}^{+2.3} \times 10^{-4}$ of the CCSN rate within $0.3 \leq z \leq 1.4$. However at redshifts $z \geq 1.5$, Cooke et al. (2012) suggested that the rate could be significantly higher, possibly as a consequence of decreasing metallicity and increasing cosmic star formation rate density. SLSN Ic may require low metallicity to be produced (e.g. Chen et al. 2013; Lunnan et al. 2014) but the efficiency of producing a SLSN from progenitor systems is still unknown and the progenitor stellar mass range is undetermined. Future surveys exploring the low, medium and high redshift distances are necessary to strengthen, or falsify, the findings here reported and hence make use of SLSN as high redshift distance probes.

Looking further ahead, detecting SLSN Ic out to redshifts of $z \simeq 10$ is quite plausible but requires space based surveys to sample the restframe 400nm and 520nm bands proposed here. As an illustration of what would be required, we plot the apparent AB magnitudes of SLSN Ic between redshifts 1 and 10 in Fig 11. These are the redshifted $M(400)$ magnitudes in the AB system, from the conventional definition

$$m_{\text{AB}} = M(400) + 5 \log(D_{\text{L}}(z)/10\text{pc}) - 2.5 \log(1+z) \quad (2)$$

where M_{AB} is the apparent AB magnitude at the redshifted wavelength and D_{L} is the luminosity distance with our chosen cosmology. We label the wavelengths and filter systems required to cover the restframe 400nm band at specific wavelengths. The magnitudes are well within the capabilities of the future EUCLID⁴ (Laureijs et al. 2011), WFIRST⁵ and James Webb Space Telescope (specifically NIRCAM⁶) missions, even out to redshifts of $z \simeq 10$. However, the luminosity distances at these redshifts are exactly what we would like to probe using our standardisation for the low redshift objects. A major uncertainty will be the rates and the numbers that these space missions may discover in their general survey and custom designed survey modes (see Tanaka et al. 2012; Cooke et al. 2012, for initial estimations of detection rates of high redshift SNe).

8. CONCLUSION

From a study of 16 well observed and well sampled SLSN Ic in the redshift range $0.1 < z < 1.2$ we have investigated their use as standard and standardizable candles. We defined two synthetic photometric wavebands and applied quantitative *K*-corrections from observed spectra to compare their magnitudes in consistent rest frame wavebands. These two wavebands are centred on 400nm (with a width of 80nm) and 520nm (with a width of 100nm) and were chosen because the spectra are con-

⁴ <http://www.euclid-ec.org>

⁵ <http://wfirst.gsfc.nasa.gov/>

⁶ <http://www.stsci.edu/jwst/instruments/nircam/>

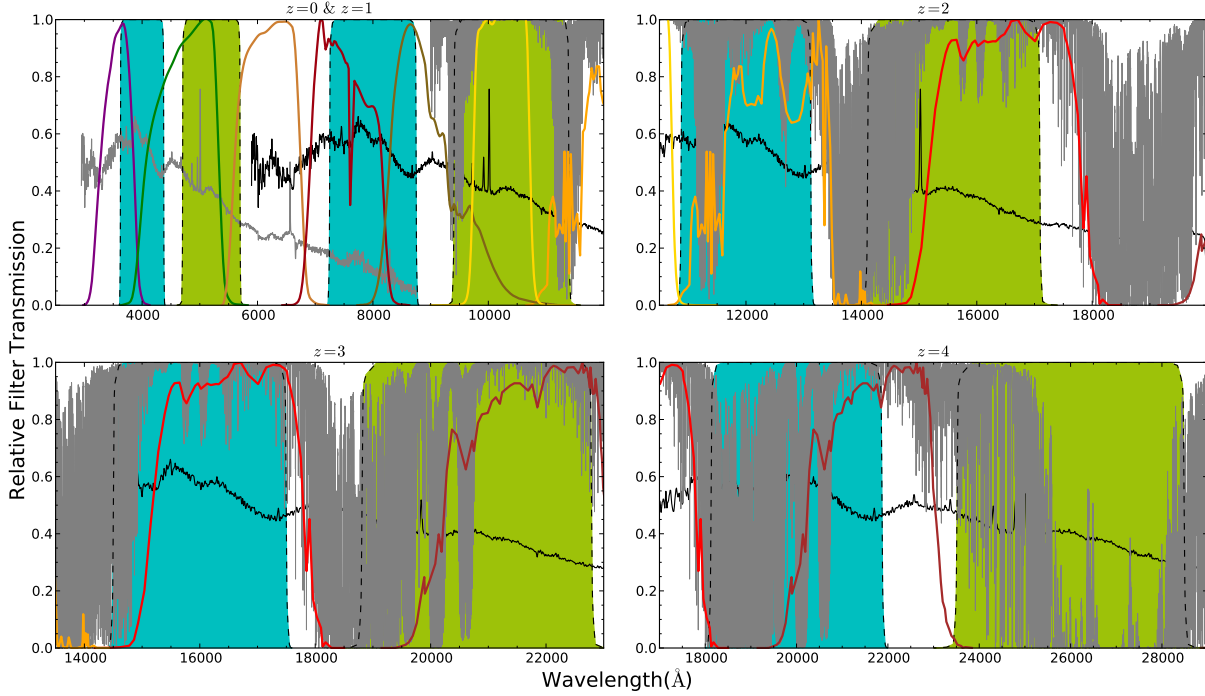


FIG. 10.— Synthetic passbands 400nm (cyan) and 520nm (green) plotted with SN2011ke spectrum at ~ 10 d scaled in flux (grey) at rest frame and at projected distances of $z = 1$ (upper left corner), $z = 2$ (upper right corner), $z = 3$ (bottom left corner) and $z = 4$ (bottom corner). Sloan u (purple) g (green), r (bronze), i (burgundy) and z (oak brown) bandpasses are displayed along the near infrared Y (gold) and the 2MASS J (orange), H (red) and K (brown) bandpasses. Also plotted in grey is the atmospheric transmission in the NIR (Lord 1992, courtesy of Gemini Observatory).

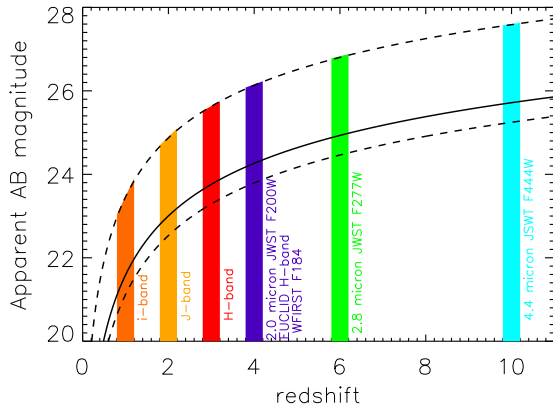


FIG. 11.— At higher redshift the only possibility of observing the 400nm and 520nm bands is using future space based telescopes. This figure illustrates the predicted AB magnitude for SLSN Ic out to $z \approx 10$. The solid line is the peak magnitude of $M(400) = -21.70$ derived here. The lower dotted line is 1σ scatter on the peak magnitudes and the upper dotted line illustrates the depth required to reach +30 days after peak, to apply the $\Delta M_{30}(400)$ correction discussed here (addition of the typical 1.4^m decline). No foreground extinction has been applied to the estimated magnitudes, since the Milky Way foreground will be minimal at these wavelengths.

tinuum dominated and relatively free from absorption features. The raw scatter of the uncorrected $M(400)$ absolute peak magnitudes is ± 0.47 mag which is immediately of interest for cosmological use, given that they have a mean peak magnitude of $M(400) = -21.70$ mag, around two magnitudes brighter than SNe Ia. We have

proposed that they can be standardized further by comparing their decline rates at +30d after peak, in the rest frame in a similar manner to the Phillips Δm_{15} relation. It appears that the fainter the SN, the faster the decline rate. **The raw scatter can be reduced to 0.25 – 0.33 mag using this $\Delta M_{30}(400)$ relation**, depending on which sample and calibration method is used.

We have also uncovered an additional method to standardize the peak magnitudes, by comparing the rest frame color evolution of SLSN. Comparison of the rate of change of color index $M(400) - M(520)$ with the peak magnitude $M(400)$ shows a **tight correlation with a very small rms scatter of 0.19–0.26 mag**. The fainter SNe are redder at peak, and they evolve to redder colors faster than their bluer and brighter counterparts. While this low rms is encouraging, we caution that it may be due to small numbers of objects since we could only use eight to ten of the SNe due to data limitations. An immediate objective is to increase the sample with enough observational data that this can be tested further.

A difficulty remains in that SLSN Ic may have distinctly different observational (or physical) sub-classes. The bulk of the population are split into two broad classes of fast evolving objects (2005ap-like) and more slowly evolving objects (2007bi-like). It is not immediately clear if these are distinct or there is a continuum of properties bridging the gap between them. The residuals of the fits in our standardizable candle methods are somewhat dependent on classification of these SLSN into these sub-classes. However the results are not critically dependent on this phenomenological classification. A further

complication is the recent discovery of a SLSN which is spectroscopically similar to the SLSN Ic, but shows additional weak $H\alpha$ emission (and hence has been classified as a SLSN type II). As it may be difficult to deselect this type of SN at high redshift from a pure sample of SLSN Ic, we included this event in our sample to check if it compromised the results. While it does appear brighter and bluer than the bulk of the SLSN Ic sample, its inclusion did not significantly increase the scatter in the $\Delta M_{30}(400)$ **relation**. It did however increase the scatter in the peak magnitude - color evolution calibration to **0.26 dex**.

The low volumetric rates of these SLSN means that they are not useful as primary distance indicators in the local Universe ($z < 0.1$). Indeed, the calibration of their peak magnitudes requires an adoption of a cosmology to determine their distance moduli at low to moderate redshift. Their usefulness may be in redshift regimes beyond those possible for SNe Ia. With current instrumentation and facilities, they have the potential to probe the Universe at $z = 2 - 4$, in which their rest frame $M(400)$ and

$M(520)$ calibration bands correspond to apparent AB magnitudes of between 23 – 24 in typical near-infrared JHK passbands. They are likely to be detectable out to redshifts of $z \simeq 10$ with future space based missions such as JWST, EUCLID and WFIRST.

We thank the anonymous referee for a careful review which improved the clarity of the paper. We wish to thank Mark Sullivan, Bob Nicholl, Andrea Pastorello, Enrico Cappellaro, Anders Jerkstrand, Morgan Fraser, Ting-Wan Chen, David Young, Stuart Sim, Rubina Kotak and Matt Nicholl for the helpful discussions. CI also thanks Robert Quimby, Ragnhild Lunnan and Stefano Benetti for providing the spectra of SN2005ap, PTF09cnd, PS1-10bj and CSS121015. CI thanks Fulvio Melia and his team for the careful reading of the paper and their suggestions. The research leading to these results has received funding from the European Research Council under the European Union’s Seventh Framework Programme (FP7/2007-2013)/ERC Grant agreement n° [291222] (PI : S. J. Smartt).

APPENDIX

DETAILS OF THE POLYNOMIAL FITTING AND INTERPOLATION OF LIGHT-CURVES

When fitting polynomials to the photometric lightcurves, we tried as far as possible to use the same time baseline: from -10 ± 5 days before maximum (in the 400nm band) to 40 ± 5 days after. The fits displayed in Figures 2 & 3 make use of this baseline and the magnitudes reported in Table 1 are those from interpolation at the specific epochs of peak, +10d, +20d and +30d, unless otherwise noted (below, we refer to these as the key epochs). Further details on each object are as follows.

- SN2010gx: This is a very well sampled SN light-curve with only two small gaps around 20 days and 27 days past maximum. We fitted 31 epochs from -8d pre-peak to 40 days after with a third order polynomial (rms = 0.06). For the key epochs we used magnitudes from interpolation, which were coincident with the measurements available specifically at epochs 0 and +10d. A polynomial of order 3 was used to fit the $M(400) - M(520)$ color curve with an rms = 0.05 in the period -5d before peak to 40 days after.
- SN2011kf: We lack specific data close to two out of four key epochs (+10d and +30d), but the light curve is extremely similar to that of SN 2010gx. The lightcurve is quite well sampled from +40d onwards (Inserra et al. 2013) and we also used these points to constraining the fit. We fitted the 6 epochs available until 45d post maximum with a second order polynomial. There is no noticeable difference between a second and third order function. We found an rms = 0.05 for the second order. If we would extend the data used out to 60 days, then the difference in the rms fit is less than 2σ . The magnitudes reported in Table 1 are derived from the fit.
- SN2011ke: This object has a well sampled g -band light-curve in the first 30d post maximum. Small gaps exist at +5d, +17d and +27d after peak. We have measurements specifically at all four key epochs and the magnitudes from interpolation are in agreement within the fit rms, hence in Table 1 we reported the actual magnitudes. An rms = 0.07 was found for a third order polynomial fit to the 19 epochs available for the baseline -17 to 31 days. If we extend the baseline up to 60 days post maximum and then include other 3 epochs, the rms for the same fit order of before increases to 0.08. We also fitted the $M(400) - M(520)$ color evolution with a third order polynomial (rms = 0.07) from -17 days before peak to 31 days after. The rms of the fit does not change if we include the following point at +51d.
- SN2012il: For this object, an observed g -band magnitude at peak is not specifically available but we do have an r -band measurement exactly at peak. To retrieve a g -band peak magnitude we used our library of template spectra at peak epoch and the observed r magnitude at peak to obtain the K -correction to the 400 nm rest frame absolute magnitude. To check the reliability of this method we also fitted the available photometry (from r to z) around peak epoch with a blackbody and then estimated the K -correction factor from r to 400 nm. The values retrieved with these two methods (template and multi-color photometry) were in agreement (see Inserra et al. 2013, for further details on these methods and their application) within an error of ~ 0.11 mag. The peak magnitude in Figure 2 is that from the spectral K -corrected method. For the g -band data available (+4d to +34d) we used a third order polynomial fit, obtaining an rms = 0.04. The fit displayed in Figure 2 does not use the peak value, but there are measurements close to the key epochs of +10, +20 and +30d. We used the same time baseline of the light curve for the $M(400) - M(520)$ color but we fitted it with a second order polynomial to avoid over fitting.

- SN2005ap: We fitted 15 epochs from -5 days from maximum to 26 days after with a third order polynomial which resulted in an $\text{rms} = 0.09$. The point at 19d past maximum was 4σ from this fit and we removed it during the fitting process in accordance with Chauvenet’s Criterion.
- PS1-10ky: This SN did not have a magnitude specifically at peak in the observed i -band (chosen for the 400nm rest frame cross-filter K -correction), however it did have r -band measurements. We fitted 15 epochs of $M(400)$ (computed from observed i -band) between $+6$ and $+36$ days after maximum with a third order polynomial ($\text{rms} = 0.07$). The values listed in Table 1 refer to magnitudes from interpolation with this fit. To check the consistency of our fit we also specifically evaluated the peak magnitude with a K -correction from the observed r -band at peak to the 400nm rest frame band, together with a spectrophotometric measurement. As in the case of SN2012il these two methods gave back similar results. The magnitude retrieved is plotted in Figure 2 and it matches the fit well. Hence we are confident that the absolute peak magnitude is reliable. While fitting the $M(400) - M(520)$ color evolution, two points at ~ 8 and ~ 22 days past maximum were rejected by application of Chauvenet’s criterion (being more than 3σ from the fit). The other points in the color evolution were fitted with a fourth order polynomial with $\text{rms} = 0.08$.
- PTF09cnd: The key epochs are available in the observed PTF09cnd light-curve. We fitted the epochs available for the -10d to $+40\text{d}$ baseline with a third order polynomial with $\text{rms} = 0.04$. The magnitudes from interpolation are in agreement with the direct measurements, and in Table 1 we report the actual magnitudes.
- SCP-06F6: The observed z -band was chosen as the filter to K -correct to retrieve the 400nm band rest frame, and the available data cover out to $\sim 20\text{d}$ past maximum. We interpolated the 6 epochs available between -30 days and 20 days from peak with a second and third order polynomial obtaining similar results. The best $\text{rms} = 0.05$ was found with the second order. As a consistency check, we also estimated what we would expect to see (assuming our fit is valid) in the i -band lightcurve at $\sim 40\text{d}$, since an i -band limit at this epoch is reported in Barbary et al. (2009). We find consistency and our z -band fit results would only be incompatible with the limit if the i -band mag would be about 1 mag fainter than the limit reported in Barbary et al. (2009). However no SLSN Ic has published data which show such a steep decrease or dramatic color change at this phase so far.
- PTF11rks: The faintest object of the sample shows two small gaps of four and five days around 11d and 23d past maximum light. We fitted the 14 observations between -3d and $+29\text{d}$ from peak with a third order polynomial obtaining $\text{rms} = 0.05$. A polynomial of equivalent order fitted the color evolution on the same baseline with $\text{rms} = 0.06$. We noticed that magnitudes from interpolation of the fits extending up to $+48$ days are in agreement with those retrieved at $+48\text{d}$ by SED fitting. The actual magnitude at peak was in agreement with that from interpolation.
- PS1-10bjz: The data cover two out of four key epochs but thanks to a sufficient coverage (8 epochs) spanning over the baseline range defined above we retrieved the best fit with a polynomial of third order and $\text{rms} = 0.07$. We also fitted the color evolution on the same baseline with a third order polynomial retrieving $\text{rms} = 0.06$.
- PS1-10pm: The data (9 epochs) cover from -4d to $+41\text{d}$. We fitted them with a third order polynomial retrieving $\text{rms} = 0.08$.
- LSQ12dlf: The key epochs are available in the observed LSQ12dlf light-curve. We fitted the 30 available epochs for our above-mentioned baseline (-10d to 40d) with a third order polynomial with 0.09 rms. The magnitudes from interpolation are in agreement with the direct measurements, and in Table 1 we report the actual magnitudes. The 12 epochs of the $M(400) - M(520)$ color evolution were fitted with a third order polynomial and 0.03 as rms.
- SN2013dg: We fitted 18 epochs from maximum to 42 days after with a third order polynomial ($\text{rms} = 0.06$). The same number of epochs were fitted for the color evolution retrieving an $\text{rms} = 0.03$.
- PTF12dam: The lightcurve is not densely sampled at peak, but we are confident about the fit results and the magnitudes at key epochs because of the slowly evolving light curve. We fitted 9 epochs from -15d to $+55\text{d}$ from peak with a third order polynomial and an $\text{rms} = 0.06$. The color evolution was also fitted in the same period with a third order polynomial and an $\text{rms} = 0.04$.
- PS1-11ap: The data coverage is good with two small gaps around 13 and 25 days after peak. A third order polynomial was used to fit the 24 data points for $M(400)$ and 20 epochs of color evolution $M(400) - M(520)$ in the range from -16d to $+42\text{d}$, retrieving $\text{rms} = 0.10$ and $\text{rms} = 0.11$, respectively. Despite the abundance of data at peak and $+30\text{d}$ from that, we used the magnitudes from interpolation to be consistent through the sample.
- CSS121015: We fitted the 24 epochs in the range -15d to $+40\text{d}$ with a third order polynomial and $\text{rms} = 0.09$. Since the light curve is likely powered by interaction (Benetti et al. 2014), especially around peak, we decided to use the actual peak magnitude instead of that from the fit, while the other values (in Table 1) come from the interpolation. We fit the color evolution in the same range of the light curve finding an $\text{rms} = 0.10$.

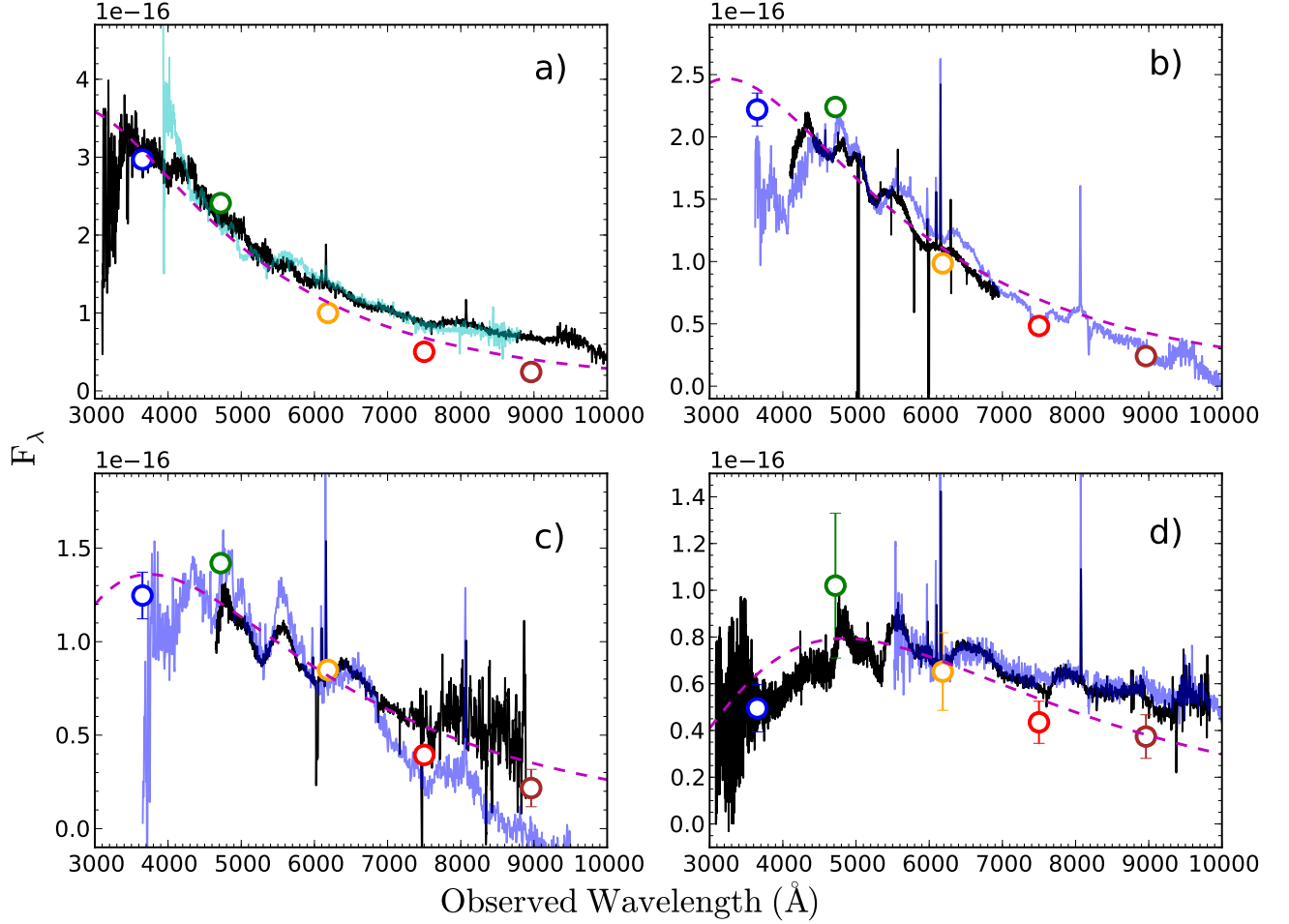


FIG. 12.— *Panel a*: observed spectrum of SN2010gx around maximum light; the SED fit (in magenta) is a blackbody fit to the *ugriz* photometry in blue, green, orange, red and brown, respectively; the template spectrum of SN2005ap at a similar epoch is plotted in cyan. *Panel b*: the same as Panel a but around +10d past maximum. The SN chosen and plotted as a template is SN2011ke (in blue). *Panel c*: same as panel b, but at +20d past maximum. *Panel d*: same as panel b, but at +30d past maximum.

TREATMENT OF ERRORS

When evaluating the errors on our absolute magnitudes, we tried as far as possible to account for all sources of error. As reported in Sec. 3.2 our observed magnitude in the passband f and absolute magnitude in the passband 400nm (the following discussion is valid also for the 520nm band) are related as follows :

$$m_f = M(400) + \mu + K_{f \rightarrow 400} + A_f . \quad (\text{B1})$$

According to the formalism reported in Blanton & Roweis (2007) the K -correction from f to 400 is the following:

$$K_{f \rightarrow 400} = -2.5 \log \left[\frac{1}{1+z} \times \frac{\int d\lambda_o \lambda_o L_\lambda(\lambda_o/1+z) f(\lambda_o) \int d\lambda_e \lambda_e g_\lambda^{400}(\lambda_e) 400(\lambda_e)}{\int d\lambda_o \lambda_o g_\lambda^f(\lambda_o) f(\lambda_o) \int d\lambda_e \lambda_e L_\lambda(\lambda_e) 400(\lambda_e)} \right] , \quad (\text{B2})$$

where L_λ is the luminosity per unit wavelength, λ_o refers to the observed frame, λ_e refers to the rest frame (e stands for emitted), g_λ^{400} is the flux density per unit wavelength for the 400nm band and g_λ^f is the same for the observed band, while $400(\lambda)$ and $f(\lambda)$ are the response of the instrument per unit photon for the rest and observed filter, respectively. Rewriting equation B1, we have :

$$M(400) = m_f - (5 \log D_L + 25) - A_f - K_{f \rightarrow 400} , \quad (\text{B3})$$

where the K -correction term is not expanded and the distance modulus has been expressed as function of distance luminosity D_L in Mpc. The errors on $M(400)$, nominally $\sigma_{M(400)}$ and equivalent to the standard deviation, are given by the combination of errors of the terms on the right hand side of equation B3. Assuming as first approximation

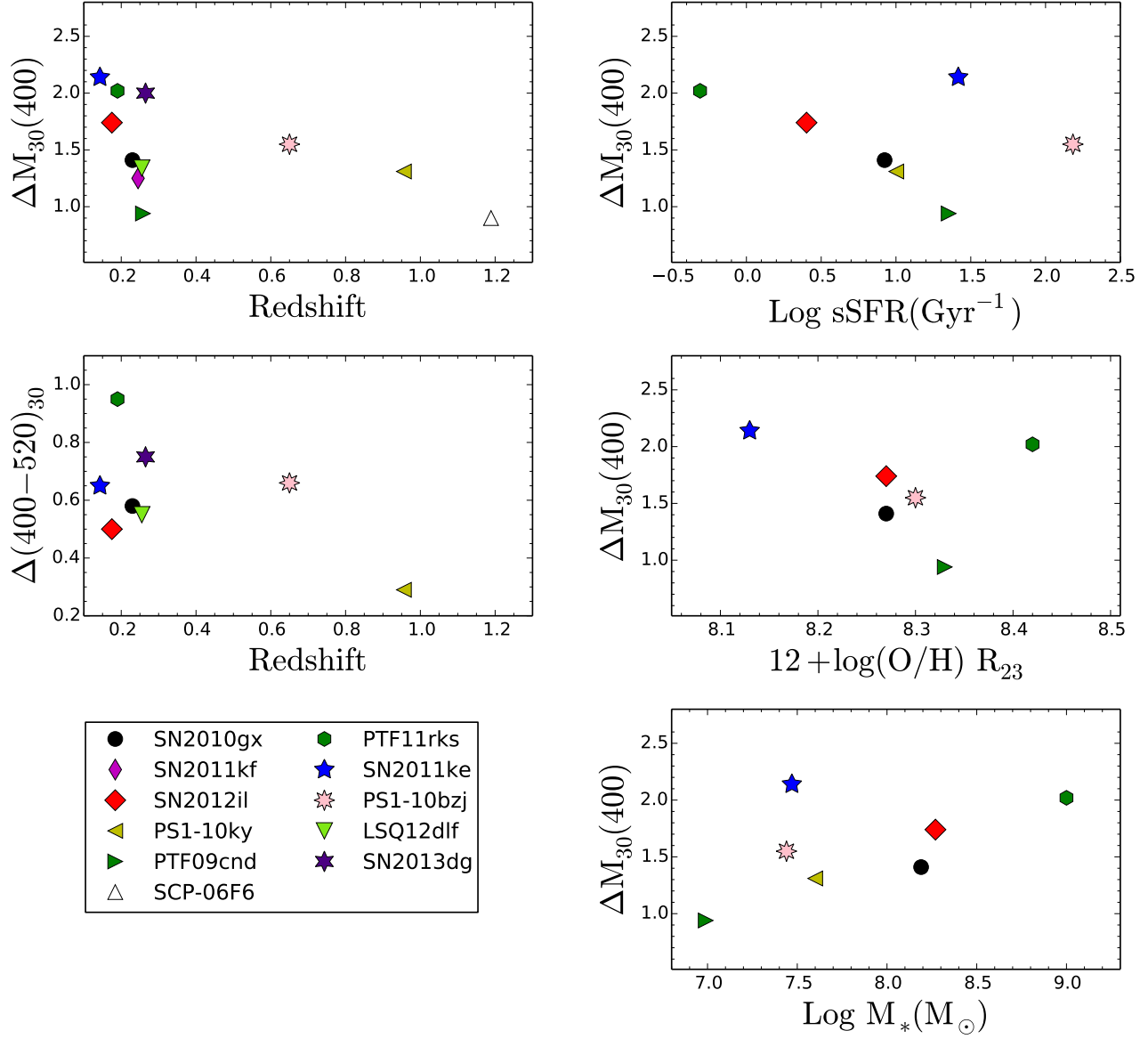


FIG. 13.— Various plots of example empirical properties of SLSN derived in this paper compared to redshift and host galaxy properties from Chen et al. (2013); Lunnan et al. (2014).

that the terms are uncorrelated and the errors deriving from the cosmology adopted are negligible, the errors on our absolute magnitude follow the equation below:

$$\sigma_{M(400)} = \sqrt{\sigma_{m_f}^2 + 4.715 \left(\frac{\sigma_{D_L}}{D_L} \right)^2 + \sigma_{A_f}^2 + 1.179 \left[\left(\frac{\sigma_z}{z} \right)^2 + \left(\frac{\sigma_{L_{\lambda_o}}}{L_{\lambda_o}} \right)^2 + \left(\frac{\sigma_{L_{\lambda_e}}}{L_{\lambda_e}} \right)^2 + \left(\frac{\sigma_{ZP_{\lambda_o}}}{ZP_{\lambda_o}} \right)^2 + \left(\frac{\sigma_{ZP_{\lambda_e}}}{ZP_{\lambda_e}} \right)^2 \right]} \quad (\text{B4})$$

Where the differences between the Vega and AB systems are taken into account by the covariance of the zero points (ZP) of the two systems (ZP_{λ_o} and ZP_{λ_e}). The two major sources of errors are related to observed magnitudes and extinction. When a cross-filter K -correction is made, the errors are usually in the range 0.005–0.05 mag (Kim et al. 1996; Blanton & Roweis 2007; Hsiao et al. 2007). These values are lower than, or comparable to, those of the errors on extinction and observed magnitudes. During our analysis we effectively always applied a cross-filter K -correction. The errors related to the K -correction can be 3–4% (0.03 – 0.04 mag) if we use two different systems for the observed and rest filter band, as we had to do for SN2005ap, PTF09cnd, LSQ12dlf and CSS121015; and can be up to 0.05 mag if the cross-filter K correction is not applied (Hsiao et al. 2007).

The error treatment so far is applicable if we use the spectrum of the SN to evaluate the K -correction. If instead of

the actual SN spectrum we use a library template spectrum (of a similar supernova) or the SED fitting (using blackbody spectra) to observed photometry then some further scatter is found but $\sigma_{M(400)}$ is not significantly affected by this. In order to quantitatively investigate the differences between the three methods, we compared the SED photometry fitting method (employing blackbody fits) and the spectral library method (using our 64 spectra) as applied to SN2010gx. We compared these values to those reported in Table 2 which were evaluated using the actual SN spectra. In Fig. 12 the three spectra used for the three methods are illustrated together. In comparison to the K -correction values derived with the SN spectra (reported in Table 2 for SN2010gx), the SED fitting method gives results which are different by 0.01–0.06 mag depending on the phase and the EW of the emission lines. The library template method results in differences which are between 0.01 to 0.05 mag, depending on the to filter and spectra used as template. We note that the major differences are found at the extremities of the optical wavelength region (e.g. u and z). These potential systematic differences were not included in the final estimates of $\sigma_{M(400)}$ (since they are not strictly speaking random errors), but are given here to quantify the differences found when using different methods for K -correction.

THE DEPENDENCE OF SLSN PROPERTIES ON THEIR HOST GALAXIES

In Figure 13 we illustrate an initial comparison of SLSN properties as a function of redshift and host galaxy properties. Two of the empirical properties determined in this paper ($\Delta M_{30}(400)$ and $\Delta(400-520)_{30}$) are plotted against redshifts and host galaxies properties from Chen et al. (2013) and Lunnan et al. (2014). The decline parameter after 30 days and the color evolution parameter are representative of the empirical properties we have investigated. The three galaxy properties used are specific star formation rate, total stellar mass and oxygen abundance. For oxygen abundance we took the R_{23} estimate from Lunnan et al. (2014), using the low metallicity branch value (since the low masses of these SLSN hosts makes this branch choice most plausible). As one might expect, from the small sample size, there is no clear dependence of SLSN properties with host galaxy properties. The two plots comparing the decline parameters with redshift illustrate that the intrinsically fainter objects are not represented at the higher redshifts, which is not unexpected given the magnitude limited surveys that the discoveries originate from. One might postulate a trend in the $\Delta M_{30}(400)$ vs $\log M_*$ plot, in the sense that the intrinsically fainter SLSN tend to occur in more massive galaxies. However this is possibly just driven by one point (either PTF09cnd at the low mass end or PTF11rks at the other mass extreme) and drawing conclusions would not be secure. Thus, an increase in the sample is mandatory in order to better investigate any underlying physical relation or redshift evolution.

REFERENCES

- Agnoletto, I., Benetti, S., Cappellaro, E., et al. 2009, ApJ, 691, 1348
- Baltay, C., Rabinowitz, D., Hadjijska, E., et al. 2013, PASP, 125, 683
- Barbary, K., Dawson, K. S., Tokita, K., et al. 2009, ApJ, 690, 1358
- Berger, E., Chornock, R., Lunnan, R., et al. 2012, ApJ, 755, L29
- Benetti S., et al., 2014, MNRAS, 441, 289
- Blanton, M. R., & Roweis, S. 2007, AJ, 133, 734
- Campana, S., Mangano, V., Blustin, A. J., et al. 2006, Nature, 442, 1008
- Cao, Y., Kasliwal, M. M., Arcavi, I., et al. 2013, ApJ, 775, L7
- Cano, Z., & Jakobsson, P. 2014, arXiv:1409.3570
- Cano, Z. 2014, arXiv:1407.2589
- Chen, T.-W., Smartt, S. J., Bresolin, F., et al. 2013, ApJ, 763, L28
- Chevalier, R. A., & Irwin, C. M. 2011, ApJ, 729, L6
- Chomiuk, L., Chornock, R., Soderberg, A. M., et al. 2011, ApJ, 743, 114
- Chornock, R., Berger, E., Rest, A., et al. 2013, ApJ, 767, 162
- Cobb B. E., Bailyn C. D., van Dokkum P. G., Natarajan P., 2006, ApJ, 645, L113
- Cooke, J., Sullivan, M., Gal-Yam, A., et al. 2012, Nature, 491, 228
- D’Andrea, C. B., Sako, M., Dilday, B., et al. 2010, ApJ, 708, 661
- Dessart, L., Hillier, D. J., Waldman, R., Livne, E., & Blondin, S. 2012, MNRAS, 426, L7
- Drake, A. J., Djorgovski, S. G., Mahabal, A. A., et al. 2011, The Astronomer’s Telegram, 3343, 1
- Drake, A. J., Djorgovski, S. G., Mahabal, A., et al. 2009, ApJ, 696, 870
- Dunkley, J., Komatsu, E., Nolta, M. R., et al. 2009, ApJS, 180, 306
- Eisenstein, D. J., Zehavi, I., Hogg, D. W., et al. 2005, ApJ, 633, 560
- Foley, R. J., Papenkova, M. S., Swift, B. J., et al. 2003, PASP, 115, 1220
- Galama, T. J., Vreeswijk, P. M., van Paradijs, J., et al. 1998, Nature, 395, 670
- Gal-Yam, A. 2012, Science, 337, 927
- Gal-Yam, A., Mazzali, P., Ofek, E. O., et al. 2009, Nature, 462, 624
- Gehrels, N. 1986, ApJ, 303, 336
- Ginzburg, S., & Balberg, S. 2012, ApJ, 757, 178
- Goldhaber G., et al., 2001, ApJ, 558, 359
- Guy, J., Astier, P., Baumont, S., et al. 2007, A&A, 466, 11
- Guy, J., Astier, P., Nobili, S., Regnault, N., & Pain, R. 2005, A&A, 443, 781
- Hamuy, M., & Pinto, P. A. 2002, ApJ, 566, L63
- Hamuy, M., Phillips, M. M., Suntzeff, N. B., et al. 1996, AJ, 112, 2438
- Hamuy, M., Phillips, M. M., Wells, L. A., & Maza, J. 1993, PASP, 105, 787
- Hogg, D. W., Baldry, I. K., Blanton, M. R., & Eisenstein, D. J. 2002, arXiv:astro-ph/0210394
- Howell, D. A., Kasen, D., Lidman, C., et al. 2013, ApJ, 779, 98
- Hsiao, E. Y., Conley, A., Howell, D. A., et al. 2007, ApJ, 663, 1187
- Hunter, D. J., Valenti, S., Kotak, R., et al. 2009, A&A, 508, 371
- Jones, D. O., Rodney, S. A., Riess, A. G., et al. 2013, ApJ, 768, 166
- Kaiser, N., et al. 2010, Proc. SPIE, 7733, 12K.
- Kasen, D., & Bildsten, L. 2010, ApJ, 717, 245
- Kim, A., Goobar, A., & Perlmutter, S. 1996, PASP, 108, 190
- Komatsu, E., Smith, K. M., Dunkley, J., et al. 2011, ApJS, 192, 18
- Kostrzewa-Rutkowska, Z., Kozłowski, S., Wyrzykowski, L., et al. 2013, ApJ, 778, 168
- King, A. L., Davis, T. M., Denney, K. D., Vestergaard, M., & Watson, D. 2014, MNRAS, 441, 3454
- Inserra, C., Smartt, S. J., Jerkstrand, A., et al. 2013, ApJ, 770, 128
- Inserra, C., Smartt, S. J., Fraser, M., et al. 2012, The Astronomer’s Telegram, 4329, 1
- Laureijs, R., Amiaux, J., Arduini, S., et al. 2011, arXiv:1110.3193
- Leloudas, G., Chatzopoulos, E., Dilday, B., et al. 2012, A&A, 541, A129
- Lord, S. D. 1992, NASA Technical Memorandum 103957
- Lunnan, R., Chornock, R., Berger, E., et al. 2014, ApJ, 787, 138
- Lunnan, R., Chornock, R., Berger, E., et al. 2013a, ApJ, 771, 97

- Maguire, K., Kotak, R., Smartt, S. J., et al. 2010, *MNRAS*, 403, L11
- Mandel, K. S., Narayan, G., & Kirshner, R. P. 2011, *ApJ*, 731, 120
- Mandel, K. S., Wood-Vasey, W. M., Friedman, A. S., & Kirshner, R. P. 2009, *ApJ*, 704, 629
- Mazzali, P. A., Valenti, S., Della Valle, M., et al. 2008, *Science*, 321, 1185
- McCrum, M., Smartt, S. J., Rest, A., et al. 2014, arXiv:1402.1631
- McCrum, M., Smartt, S. J., Kotak, R., et al. 2014, *MNRAS*, 2595
- McKenzie, E. H., & Schaefer, B. E. 1999, *PASP*, 111, 964
- Mirabal, N., Halpern, J. P., An, D., Thorstensen, J. R., & Terndrup, D. M. 2006, *ApJ*, 643, L99
- Modjaz, M., Li, W., Butler, N., et al. 2009, *ApJ*, 702, 226
- Nicholl, M., Smartt, S. J., Jerkstrand, A., et al. 2013, *Nature*, 502, 346
- Nicholl, M., Smartt, S. J., Jerkstrand, A., et al. 2014, *MNRAS*, 444, 2096
- Nugent, P., Sullivan, M., Ellis, R., et al. 2006, *ApJ*, 645, 841
- Nugent, P., Kim, A., & Perlmutter, S. 2002, *PASP*, 114, 803
- Oke, J. B., & Sandage, A. 1968, *ApJ*, 154, 2
- Pandey, S. B., Anupama, G. C., Sagar, R., et al. 2003, *MNRAS*, 340, 375
- Pastorello, A., Smartt, S. J., Botticella, M. T., et al. 2010, *ApJ*, 724, L16
- Pastorello, A., Smartt, S. J., Kankare, D., et al. 2010, *The Astronomer's Telegram*, 2504, 1
- Pastorello, A., Kasliwal, M. M., Crockett, R. M., et al. 2008, *MNRAS*, 389, 955
- Patat, F., Cappellaro, E., Danziger, J., et al. 2001, *ApJ*, 555, 900
- Patat, F., Chandra, P., Chevalier, R., et al. 2007, *Science*, 317, 924
- Percival, W. J., Reid, B. A., Eisenstein, D. J., et al. 2010, *MNRAS*, 401, 2148
- Perlmutter, S., Gabi, S., Goldhaber, G., et al. 1997, *ApJ*, 483, 565
- Phillips, M. M. 1993, *ApJ*, 413, L105
- Pian, E., Mazzali, P. A., Masetti, N., et al. 2006, *Nature*, 442, 1011
- Poznanski, D., Butler, N., Filippenko, A. V., et al. 2009, *ApJ*, 694, 1067
- Prieto, J. L., Drake, A. J., Mahabal, A. A., et al. 2012, *The Astronomer's Telegram*, 3883, 1
- Prieto, J. L., Rest, A., & Suntzeff, N. B. 2006, *ApJ*, 647, 501
- Pskovskii, I. P. 1977, *Soviet Ast.*, 21, 675
- Quimby, R. M., Oguri, M., More, A., et al. 2014, *Science*, 344, 396
- Quimby, R. M., Yuan, F., Akerlof, C., & Wheeler, J. C. 2013, *MNRAS*, 431, 912
- Quimby, R. M., Werner, M. C., Oguri, M., et al. 2013, *ApJ*, 768, L20
- Quimby, R. M., Kulkarni, S. R., Kasliwal, M. M., et al. 2011, *Nature*, 474, 487
- Quimby, R. M., Gal-Yam, A., Arcavi, I., et al. 2011, *The Astronomer's Telegram*, 3841, 1
- Quimby, R. M., Sternberg, A., & Matheson, T. 2011, *The Astronomer's Telegram*, 3344, 1
- Quimby, R. M., Kulkarni, S. R., Ofek, E., et al. 2010, *The Astronomer's Telegram*, 2492, 1
- Quimby, R. M., Aldering, G., Wheeler, J. C., et al. 2007, *ApJ*, 668, L99
- Quimby, R. 2006, *Central Bureau Electronic Telegrams*, 644, 1
- Quimby, R. M., Castro, F., Gerardy, C. L., et al. 2005, *Bulletin of the American Astronomical Society*, 37, #171.02
- Rau, A., Kulkarni, S. R., Law, N. M., et al. 2009, *PASP*, 121, 1334
- Richmond, M. W., van Dyk, S. D., Ho, W., et al. 1996, *AJ*, 111, 327
- Riess, A. G., Filippenko, A. V., Challis, P., et al. 1998, *AJ*, 116, 1009
- Riess, A. G., Press, W. H., & Kirshner, R. P. 1996, *ApJ*, 473, 88
- Rodney, S. A., Riess, A. G., Dahlen, T., et al. 2012, *ApJ*, 746, 5
- Rust, B. W. 1974, *BAAS*, 6, 309
- Smith, N., Li, W., Foley, R. J., et al. 2007, *ApJ*, 666, 1116
- Smith, N., & McCray, R. 2007, *ApJ*, 671, L17
- Soderberg, A. M., Berger, E., Page, K. L., et al. 2008, *Nature*, 453, 469
- Sollerman, J., Jaunsen, A. O., Fynbo, J. P. U., et al. 2006, *A&A*, 454, 503
- Sollerman, J., Kozma, C., Fransson, C., et al. 2000, *ApJ*, 537, L127
- Stritzinger, M., Mazzali, P., Phillips, M. M., et al. 2009, *ApJ*, 696, 713
- Suzuki, N., Rubin, D., Lidman, C., et al. 2012, *ApJ*, 746, 85
- Tanaka, M., Moriya, T. J., Yoshida, N., & Nomoto, K. 2012, *MNRAS*, 422, 2675
- Tomita, H., Deng, J., Maeda, K., et al. 2006, *ApJ*, 644, 400
- Tonry, J. L., Stubbs, C. W., Lykke, K. R., et al. 2012, *ApJ*, 750, 99
- Valenti, S., Fraser, M., Benetti, S., et al. 2011, *MNRAS*, 416, 3138
- Valenti, S., Benetti, S., Cappellaro, E., et al. 2008, *MNRAS*, 383, 1485
- Valenti, S., Elias-Rosa, N., Taubenberger, S., et al. 2008, *ApJ*, 673, L155
- Woosley, S. E. 2010, *ApJ*, 719, L204
- Yoshii, Y., Tomita, H., Kobayashi, Y., et al. 2003, *ApJ*, 592, 467
- Young, D. R., Smartt, S. J., Valenti, S., et al. 2010, *A&A*, 512, A70